이학석사 학위논문

빛을 조사하여 증가된 촉매성과 구조를 가진 실리카 코팅된 금 나노막대에 대한 연구

Light Treatment of Silica-Coated Gold Nanorods to Have Enhanced Catalytic Performances and Structures

2014년 2월

서울대학교 대학원

화학부 물리화학 전공

손 명 희

Light Treatment of Silica-Coated Gold Nanorods to Have Enhanced Catalytic Performances and Structures

by Myounghee Son

Supervisor: Professor Du-Jeon Jang

Major: Physical Chemistry

Department of Chemistry

Graduate School of

Seoul National University

February 2014

빛을 조사하여 증가된 촉매성과 구조를 가진 실리카 코팅된 금 나노막대에 대한 연구

Light Treatment of Silica-Coated Gold Nanorods to Have Enhanced Catalytic Performances and Structures

지도교수 장 두 전

이 논문을 이학석사 학위논문으로 제출함
2013년 12월

서울대학교 대학원
화학부 물리화학 전공
손 명 희

손명희의 이학석사 학위논문을 인준함
2013년 12월

위 원 장 강 헌 (서명)

부위원장 장 두 전 (서명)

위 원 민 달 희 (서명)

Abstract of Dissertation

The optical, structural, and catalytic properties of silica-coated gold nanorod structures treated by light have been investigated using the time-dependent and static UV-Vis absorption spectroscopy and electron microscopy.

Chapter 1 describes the enhanced catalytic performances of light-treated mesoporous silica-coated gold nanorods via the reduction of 4-nitrophenol in the presence of sodium borohydride. The light treatment of mesoporous silica-coated gold nanorods prior to catalytic experiments improves the catalytic activity of the nanocatalyst extensively without deteriorating the encapsulation effect of mesoporous silica that enhances the stability and reusability of the nanocatalyst by preventing the aggregation and dissolution of gold nanorods. Irradiation increases the catalytic rate constant largely with reducing the activation energy and the induction time of the catalytic reaction substantially; surface atom restructuring induced by photothermal annealing during irradiation has rendered the metallic surface to adsorb reactants easily and to facilitate rapid electron relays from BH_4^- to 4-nitrophenol, lowering the kinetic barrier of the catalytic reaction considerably.

Chapter 2 presents laser-induced welding of linearly assembled gold nanostructures to fabricate silica-coated gold nanowire structures using the nanosecond laser. Self-assembled chains of end-to-end linked gold nanorods can be fabricated in isopropanol solution in the absence of linker molecules. End-to-end assembled gold nanorods could be directly encapsulated with silica in mixture solution of IPA and aqueous colloids of gold nanorods. In order for the assembly to have electrical ohmic contact, the assemblies of gold nanorods are irradiated by nanosecond laser and welded to have nanoconjunction, producing gold

nanowire structures. The thermalized photon energy of surface-plasmon excitation of coupled gold nanochains has induced gold nanorods to electrically weld together within silica shells, generating silica-coated gold nanowires.

Keywords: Catalysis, Core-shell, Gold, Laser welding, Light treatment, Nanorod, Noble-metal, Self-assembly

Student Number: 2011-20295

Contents

List of Figures and Tables

reduction cycles via 9 pM of (squares) irradiated Au@mSiO$_2$ NRs and (circles) Au@CTAB NRs in the presence of $NaBH_4$.

Table 1-1. Rate constants, induction times, frequency factors, activation energies, and activation entropies for the catalytic degradation of 4-nitrophenol via nanocatalysts in the presence of $NaBH_4$.

Figure 2-1. Schematic for the fabrication of a silica-coated gold nanowire.

Figure 2-2. (a) TEM image and (b) HRTEM image of a gold nanowire. Nanowelding of silica-coated gold nanorods on a TEM grid has been carried out by 6 ns laser pulses of 1064 nm for 5 min at fluence of 0.38 mJ cm^{-2}.

Figure 2-3. STEM images and corresponding EDX elemental maps of (a) a silica-coated gold nanochain and (b) a silica-coated gold nanowire.

Figure 2-4. Area-normalized EDX elemental profiles of (a) a silica-silica coated gold nanochain and (b) a silica-coated gold nanowire scanned along the lines in the STEM images of the insets.

Figure 2-5. TEM images of (a) gold nanorods and (b) gold nanochains. (c) Extinction spectra of 0.5 mL gold NR colloid recorded as a function of time indicated in the units of min after adding 2.5 mL isopropanol. The arrows indicate the direction of time increase.

Figure 2-6. (a) Typical low-magnification TEM image of silica-coated gold nanochains. (b) Extinction spectrum of the nanochains suspended in ethanol.

Figure 2-7. TEM images of silica-coated gold nanochains with shell thickness values of (a)

20 nm, (b) 35 nm, and (c) 55 nm. Each scale bar indicates 50 nm.

Chapter 1. Light-Treated Silica-Coated Gold Nanorods Having Highly Enhanced Catalytic Performances and Reusability

1.1. Abstract

A simple post-treatment method of irradiation with a Xe lamp for 2 h has been observed to enhance the catalytic performances of a nanocatalyst on a large scale. The light treatment of mesoporous silica-coated gold nanorods having an average diameter of 17.5 nm and a typical aspect ratio of 4 with a uniform shell thickness of 20 nm improves the catalytic activity of the nanocatalyst for the reduction of 4-nitrophenol in the presence of $NaBH_4$ extensively without deteriorating the encapsulation effect of mesoporous silica that enhances the stability and reusability of the nanocatalyst by preventing the aggregation and dissolution of gold nanorods. Irradiation increases the catalytic rate constant largely with reducing the activation energy and the induction time of the catalytic reaction substantially; surface atom restructuring induced by photothermal annealing during irradiation has rendered the metallic surface to adsorb reactants easily and to facilitate rapid electron relays from BH_4^- to 4-nitrophenol, lowering the kinetic barrier of the catalytic reaction considerably.

1.2. Introduction

Nanostructured materials with functional properties have been widely explored as they can be employed potentially in a diverse range of technologies [1,2]. In particular, the control of the sizes, shapes, and compositions of noble-metal nanostructures has been broadly studied for applications such as catalysts, optoelectronics, and biomedicines [3,4]. Unique properties of noble-metal nanoparticles compared with bulk metals, due to their quantum effects and extremely high surface-to-volume ratios, facilitate catalytic performances in synthesis reactions [5]. Among the nanostructures of noble metals, gold nanoparticles have attracted widespread interest in the field of nanocatalysis as gold exhibits unique catalytic activity for important chemical reactions such as selective reduction and oxidation reactions [6-8].

The reduction of 4-nitrophenol (4NP) by $NaBH_4$ to form 4-aminophenol has been used as a model reaction to estimate the catalytic performances of noble metal nanoparticles [9-11]. The reduction mechanism of 4NP has been demonstrated based on the Langmuir-Hinshelwood model in previous reports [9,12] that the catalytic reaction takes place when both of the electron donor BH_4^- and the electron acceptor 4NP are adsorbed onto a catalyst surface. Zeng et al. [10] have compared the catalytic activities of gold-based nanocages, nanoboxes, and nanoparticles in the reduction of 4NP, suggesting that a high surface area enhances catalytic efficiency. So far, although a few studies have been reported about the catalytic reactivity of gold nanorods [5,11], their stability and reusability have been hardly reported yet. Bai et al. [11] have studied the dependence of catalytic performances on the aspect ratios of gold nanorods, revealing that short gold nanorods have excellent catalytic efficiency.

For catalytic applications, nanoparticles need to be highly stable against the surrounding medium, heat, and recycling while being catalytically active. The surface of gold nanorods (NRs) is often surrounded by the surfactant of cetyltrimethylammonium bromide (CTAB). Positively charged gold NRs surrounded by a CTAB bilayer are prevented from their aggregation in an aqueous solution via electrostatic repulsion [13]. However, in the case of an organic solution, the desorption of CTAB into the surrounding medium can induce the aggregation of CTAB-stabilized gold nanorods (Au@CTAB NRs), losing their catalytic properties. Also, due to higher surface-to-volume ratios, Au@CTAB NRs are thermodynamically unstable and tend to reduce their surface energy, transforming into spherical nanostructures [14]. To overcome the aforesaid disadvantages, it is necessary to design stable and reactive nanocatalysts by coating an additional material on the surface of gold NRs to lower the overall price of the noble-metal nanocatalysts. In principle, the shell-coating method should be straightforward to form a deposit on the surface of a catalyst and to give chemical and thermal stability to the catalyst, ensuring the reuse of the catalyst after a reaction. The shell structure should not hinder reactants from access to the catalyst surface in order to preserve catalytic reactivity. For example, nonporous shells generally result in separation between the core surface and its solvent environment [15,16], making it difficult for outside reactants to diffuse in and out [17]. However, a porous shell, especially mesoporous silica, does not cover the entire active surface of a nanocatalyst, enabling reactants to penetrate through pores [15-21]. A mesoporous silica shell has many advantages. First, the silica shell provides high stability in tough conditions such as heat, solvent exchange, and centrifugation. Moreover, it does not deteriorate the optical properties of the core noble-metal nanoparticle because silica is transparent in the visible. Last, mesoporous silica shells have large pore volumes so that reactant molecules can diffuse through pores into

the surface of catalysts [22,23]. For the first time, Gorelikov et al. [16] have reported a method to coat mesoporous silica on Au@CTAB NRs directly without having any intermediary coating step. Gold nanorods with a mesoporous silica shell have attracted numerous interests in diverse fields such as bioimaging and photothermal therapy [13,23,24]. However, the catalytic performances of mesoporous silica-coated gold nanorods (Au@mSiO_2 NRs) have not been studied so far.

In this paper, we have demonstrated a facile and effective post-treatment strategy to enhance the catalytic performances of Au@mSiO_2 NRs highly by simply irradiating light to the colloidal solution. First of all, we have synthesized gold nanorods and coated them with mesoporous SiO_2 to provide stability for the metallic nanocatalysts. Then, Au@mSiO_2 NRs have been irradiated by a Xe lamp for 2 h. Finally, we have chosen the reduction of 4-nitrophenol with $NaBH_4$ to produce 4-aminophenol as a model reaction to investigate the catalytic efficiencies of Au@CTAB NRs, Au@mSiO_2 NRs, and irradiated Au@mSiO_2 NRs. It is found that the nanocatalyst of irradiated Au@mSiO_2 NRs exhibits highly enhanced catalytic performances as well as excellent catalytic reusability.

1.3. Experimental Section

Chemicals. Ascorbic acid (s, 99.9%), CTAB (s, 96%), $HAuCl_4 \cdot 3H_2O$ (s, 99.9%), 37% HCl(aq), methanol(*l*), 4-nitrophenol (s, ≥99%), $AgNO_3$ (s, ≥99%), $NaBH_4$ (s, 96%), NaOH (s, ≥98%), and tetraethyl orthosilane (TEOS, *l*, ≥99%) were used as purchased from Sigma-Aldrich. Ultrapure deionized water (>17 MΩ cm) was obtained using a Millipore Milli-Q system.

Preparation of Gold Nanorods. Au@CTAB NRs were synthesized using a seed-mediated and CTAB-assisted method [25]. 0.25 mL of 10 mM $HAuCl_4$(aq) was added to 9.75 mL of 0.10 M CTAB(aq) with gentle shaking for 10 s. Then, 0.60 mL of freshly prepared ice-cold 10 mM $NaBH_4$(aq) was added quickly to the mixture solution under vigorous stirring for 2 min. This seed solution was kept in a 27 ˚C water bath for at least 2 h before further use. 3.0 mL of 10 mM $HAuCl_4$(aq) and 0.40 mL of 10 mM $AgNO_3$(aq) were first mixed with 40 mL of 0.10 M CTAB(aq). 0.80 mL of 1.0 M HCl(aq) was added to adjust the pH of the growth solution, and 0.32 mL of 0.10 M ascorbic acid(aq) was then added to the mixture. After the growth solution was shaken gently, 96 μL of the gold seed solution was added. The mixed solution was gently mixed and then left undisturbed overnight at 27 ˚C. The aqueous colloidal solution of as-synthesized gold nanorods was centrifuged at 8500 rpm for 8 min, the supernatant was discarded carefully, and the precipitates were dispersed in 16 mL of water. The centrifugation and dispersion processes were repeated. The concentration of CTAB in the finally purified gold colloidal solution was estimated to be 0.12 mM. During centrifugation, temperature was maintained at 26~30 ˚C to prevent the crystallization of CTAB in the solution.

Preparation of Mesoporous Silica-Coated Gold Nanorods. Mesoporous silica coating was performed according to the previously published procedures [16,24] with some modifications. 30 μL of 0.10 M CTAB(aq) was added to 3.0 mL of the gold colloidal solution described above and stirred for 30 min at 27 ˚C. Then, 30 μL of 0.10 M NaOH(aq) was added with vigorous stirring and then 30 μL of 20% TEOS in methanol was injected under gentle stirring three times at a 30 min interval. The mixture was allowed to react under gentle stirring for 24 h. The resultant solution was centrifuged and washed with ethanol repeatedly, and then the precipitate of Au@mSiO_2 NRs was dispersed in 3.0 mL of water.

Irradiation of a Xe Lamp to Mesoporous Silica-Coated Gold Nanorods. The colloidal solution of as-prepared Au@mSiO_2 NRs containd in a cuvette having a path length of 2 mm were irradiated with a 300 W Xe lamp for 2 h at room temperature to produce irradiated Au@mSiO_2 NRs. The cuvette was 10 cm away from the light source and the entire face of the sample facing the light source (1 cm × 3 cm) was uniformly irradiated by the Xe lamp. To prevent the sample from evaporation, the top of the cuvette was sealed with paraffin film.

Catalysis Experiment. The catalytic properties of gold NRs were measured by monitoring the reduction reaction of 4-nitrophenol in the presence of $NaBH_4$ [26]. 0.12 mL of 2.0 mM 4-nitrophenol(aq) was diluted with 1.6 mL of water in a polyphenyl cell having a path length of 10 mm, and then 0.30 mL of a colloidal diluted solution containing Au@CTAB NRs, Au@mSiO_2 NRs, or irradiated Au@mSiO_2 NRs was added, making the final concentration of a nanocatalyst as 13 pM (2.6 ng L^{-1}). The resulting solution was shaken gently and 2.0 mL of ice-cold 60 mM $NaBH_4$(aq) was added at once. Then, the absorption spectral changes of 4-nitrophenol were measured at scheduled intervals using a temperature-controllable

spectrophotometer. The concentration of gold nanorods was estimated using the wavelengths at the surface-plasmon maximum and the associated extinction coefficient of gold NRs obtained from an optical spectrum [27]. We have assumed that the concentration of gold nanorods remains invariant during the silica coating process. So, the concentration of gold nanorods in each as-prepared colloidal solution of Au@CTAB NRs or Au@mSiO_2 NRs was found to be 0.63 nM. 1.0 mL of each as-prepared colloidal solution was diluted by adding 2.5 mL of water to be used as a nanocatalyst. To study the reusability of nanocatalysts, used gold NRs were separated from the reaction mixture by centrifugation (13000 rpm, 3 min) at the end of each run and then re-dispersed in water.

Characterization. Transmission electron microscopic (TEM) images were obtained by a Hitachi H-7600 microscope. High-resolution TEM (HRTEM) and scanning TEM (STEM) images and energy-dispersive X-ray (EDX) line-scanned elemental intensity profiles were measured by a JEOL JEM-2100F microscope. UV/vis absorption spectra were measured using a temperature-controllable Scinco S-3000 spectrophotometer.

1.4. Results and Discussion

1.4.1. Preparation of Mesoporous Silica-Coated Au NRs

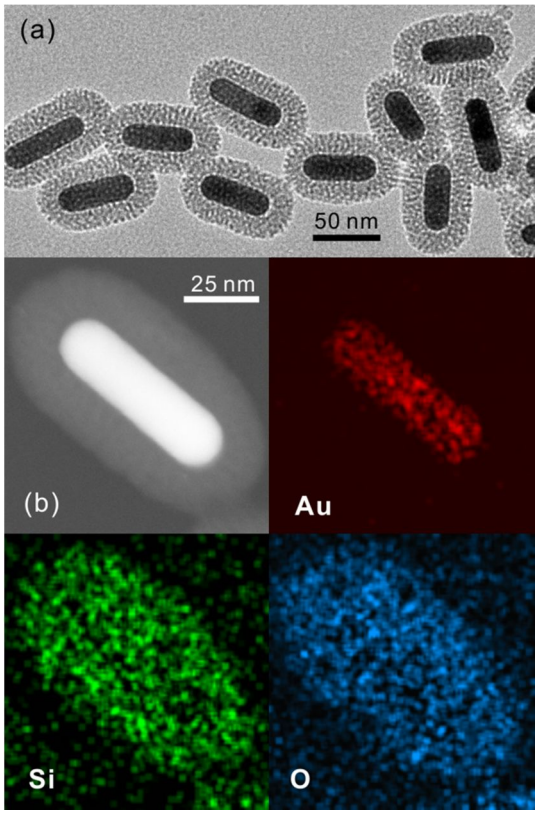

Figure 1-1. (a) TEM image of Au@mSiO$_2$ NRs and (b) STEM image and EDX elemental maps of a Au@mSiO$_2$ NR.

CTAB-stabilized Au NRs (Au@CTAB NRs) with an average diameter of 17.5 ± 0.2 nm and an average aspect ratio of about 4 were synthesized via the seed-mediated method [25]. The as-synthesized solution of Au@CTAB NRs was centrifuged twice to remove excess CTAB, leaving enough CTAB behind to prevent gold nanorods from aggregation. As-synthesized Au@CTAB NRs in our experiment exhibit a molar extinction coefficient of 5.3 × 10^{-9} M^{-1} cm^{-1} at 835 nm [27]; the concentration of Au@CTAB NRs in the as-prepared

colloidal solution was calculated to be 0.63 nM and the average number of gold atoms in a gold nanorod was estimated to be 9.1×10^5. Au@CTAB NRs have been coated with mesoporous silica to improve the structural stability and the reusability of gold nanorods. Fig. 1a shows that gold nanorods have been coated with mesoporous silica with a typical thickness of 20 nm; disordered mesopores are clearly visible in the TEM image. The low-magnification TEM image of Fig. S1 in Supporting Information also shows clearly that all the gold NRs were individually and uniformly coated by mesoporous silica. The STEM image and the EDX elemental maps of Fig. 1b support the above description of Au@mSiO_2 NRs as well. The core of a Au@mSiO_2 NR consists of gold atoms while the shell of the nanostructure is composed of silicon and oxygen atoms.

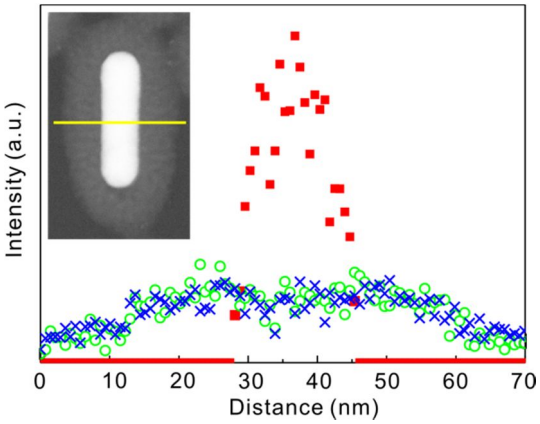

Figure 1-2. Area-normalized EDX elemental profiles of a Au@mSiO_2 NR scanned along the line in the STEM image of the inset. Squares indicate Au while circles and crosses do Si and O, respectively.

The EDX elemental profiles of a Au@mSiO_2 NR scanned along the indicated solid line of the insetted STEM image in Fig. 2 show that gold is present at the core of the nanostructure whereas silica consisting of silicon and oxygen atoms surrounds the gold core.

The shapes of the intensity profiles of elements Si and O suggest that the gold nanorod is coated homogeneously by a mesoporous silica shell. It has been reported that the CTAB concentration in the aqueous colloid of Au NRs affects silica coating [28,29] because positively charged CTAB on a Au NR serves as a template for the hydrolysis of TEOS and thus helps to form a mesoporous silica layer onto the surface of a Au@CTAB NR [16]. By carefully examining the volume ratio of the centrifuged pellet to the supernatant of the as-synthesized colloidal solution, the CTAB concentration was estimated to be 0.12 mM. Then, additional 30 μL of 0.10 M CTAB(aq) was added to 3.0 mL of the aqueous colloid of Au@CTAB NRs to keep sufficient CTAB at the surface, which acts as a template for successful mesoporous-silica deposition. In our experiment, if silica was tried to deposit onto gold nanorods without adding additional CTAB, gold nanorods were aggregated within 30 min after the first addition of TEOS. If the CTAB concentration in the colloidal solution was too high, gold-free aggregated particles of mesoporous silica were also produced (Fig. S2 in Supporting Information). Therefore, it is important to control the CTAB concentration precisely for the proper coating of mesoporous silica onto Au@CTAB NRs.

1.4.2. Light Treatment of Au@mSiO$_2$ NRs

An aqueous colloidal solution of as-prepared Au@mSiO$_2$ NRs contained in a cuvette having a path length of 2 mm has been irradiated at room temperature for 2 h by a 300 W Xe lamp to produce irradiated Au@mSiO$_2$ NRs. The TEM and STEM images and the EDX elemental maps of irradiated Au@mSiO$_2$ NRs in Fig. S3 in Supporting Information, as well as the EDX spectra of Fig. S4 in Supporting Information, indicate that neither the structure nor the composition of Au@mSiO$_2$ NRs has been changed apparently by light treatment although their catalytic performances have been improved greatly (see below). Thus, this also

supports that mesoporous-silica coating protects Au NRs from structural and compositional deformation.

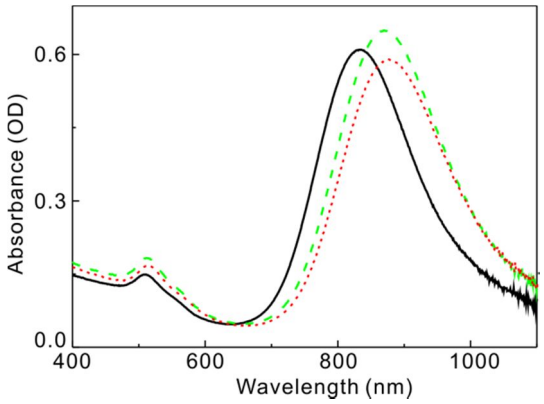

Figure 1-3. Absorption spectra of (solid) Au@CTAB NRs, (dotted) Au@mSiO$_2$ NRs, and (dashed) irradiated Au@mSiO$_2$ NRs suspended in water.

Fig. 3 shows that the wavelength at the surface-plasmon maximum (λ_{max}) of Au@mSiO$_2$ NRs (880 nm) is shifted to the red by 45 nm from the λ_{max} of Au@CTAB NRs (835 nm), indicating that silica coating affects the localized surface-plasmon resonances of Au NRs significantly. The red shift of λ_{max} with silica coating has been attributed to the increase of the refractive index of the surrounding medium [23,30]; the refractive indices of water and silica are 1.33 and 1.45, respectively. On the other hand, the λ_{max} of irradiated Au@mSiO$_2$ NRs (875 nm) is shifted to the blue by 5 nm from the λ_{max} of Au@mSiO$_2$ NRs. This slight blue shift suggests that the aspect ratios of mesoporous silica-coated gold nanorods have been decreased very slightly by the photothermal annealing effect of gold nanorods during light irradiation. Nonetheless, Fig. 3 also supports that light treatment has hardly changed the apparent structure of Au@mSiO$_2$ NRs.

1.4.3. Catalytic Performances

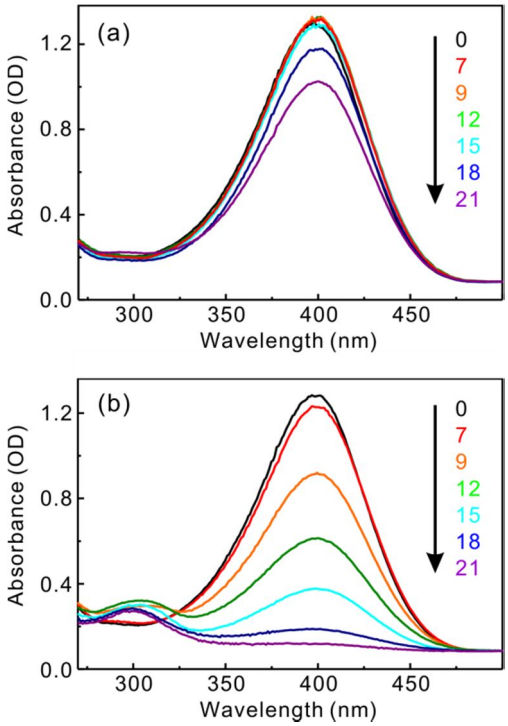

Figure 1-4. Absorption spectra at 25 ˚C of 69 μM 4-nitrophenol(aq) in the presence of 33 mM $NaBH_4$ after addition of (a) Au@mSiO_2 NRs and (b) irradiated Au@mSiO_2 NRs to be 13 pM, measured at elapsed times indicated in the units of min.

We have investigated the catalytic performances of three different nanocatalysts of Au@CTAB NRs, Au@mSiO_2 NRs, and irradiated Au@mSiO_2 NRs by monitoring time-dependent absorbance changes of 4-nitrophenol(aq) in the presence of $NaBH_4$. This catalytic reduction study is important from the industrial point of view because nitroaromatic compounds are known as the most toxic and refractory pollutants. In contrast to their toxicity in water, they are extensively produced by industrial organic reactions to synthesize dyes, pesticides, and explosives [31-33]. The absorption peak of 4-nitrophenol shifts from 317 to 400 nm due to the formation of 4-nitrophenolate ions in an alkaline condition caused by the

addition of $NaBH_4$(aq). After nanocatalysts were added, the catalytic conversion of 4-nitrophenolate ions to 4-aminophenol with increasing time was monitored as a gradual decrease of the absorption peak at 400 nm and the appearance of a new absorption peak at 300 nm. Fig. 4 reveals that the catalytic activity of irradiated Au@mSiO_2 NRs is much more efficient than that of Au@mSiO_2 NRs. The absorbance of 4-nitrophenolate(aq) at 400 nm has been found to decrease much more rapidly in the presence of irradiated Au@mSiO_2 NRs (Fig. 4b) than in the presence of Au@mSiO_2 NRs (Fig. 4a). Whereas the catalytic reaction via irradiated Au@mSiO_2 NRs was completed within 21 min, only 21% of the dye was reduced catalytically via Au@mSiO_2 NRs.

During the catalytic reduction reaction, the concentration ratio of $NaBH_4$ to 4-nitrophenol was kept high to ensure that pseudo-first-order kinetic conditions could be applied to obtain reaction rate constants [26]. Hence, Fig. 5 shows good linear relationships between $\ln(A_t/A_0)$ and the reaction time, where A_t and A_0 are the absorbance of 4-nitrophenolate(aq) at the times t and 0, respectively. Fig. 5 also demonstrates that after a certain time, called the induction time (t_0), the reaction follows pseudo-first-order kinetics and the slope of the straight line gives the rate constant of the catalytic reaction. In the absence of nanocatalysts, the thermodynamically favorable reduction of 4-nitrophenolate has not been observed to take place and the absorption peak due to 4-nitrophenolate ions at 400 nm has remained unchanged even in a couple of days, even though BH_4^-(aq) is known to be a strong reducing agent (E_0 for 4-nitrophenol/4-aminophenol = -0.76 V and H_3BO_3/BH_4^- = -1.33 V versus NHE) [34]. The rate constants of reactions carried out at four different temperatures have been calculated from the slopes of the straight lines of Fig. 5, revealing that as the reaction temperature increases, the catalytic performances of nanocatalysts become enhanced (Table 1). Fig. 5 and Table 1 reveal that the catalytic rate constant and the induction time of

irradiated Au@mSiO$_2$ NRs are substantially larger and shorter than the respective ones of Au@mSiO$_2$ NRs (see below).

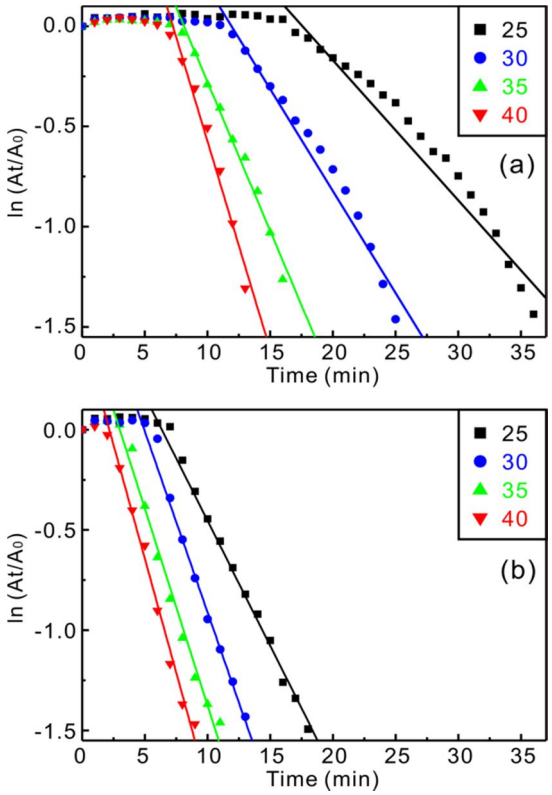

Figure 1-5. First-order kinetics, ln (A_t/A_0) vs t, for the catalytic reduction of 4-nitrophenol(aq) via 13 pM nanocatalysts of (a) Au@mSiO$_2$ NRs and (b) irradiated Au@mSiO$_2$ NRs in the presence of $NaBH_4$ at temperatures indicated in the units of ˚C.

From Fig. 6, activation energies (Ea) values of 6.5, 12.9, and 7.4 kcal mol^{-1} have been obtained for the reduction reaction of 4-nitrophenolate(aq) catalyzed by 13 pM of Au@CTAB NRs, Au@mSiO$_2$ NRs, and irradiated Au@mSiO$_2$ NRs, respectively (Table 1). The Ea value with Au@CTAB NRs is close to that of Au nanocages (6.7 kcal mol^{-1}) with high catalytic activity [10]. The Ea value with irradiated Au@mSiO$_2$ NRs (7.4 kcal mol^{-1}) is much smaller than that with Au@mSiO$_2$ NRs (13.1 kcal mol^{-1}); it is rather close to that with Au@CTAB

NRs. This implies that light irradiation to Au@mSiO$_2$ NRs lowers the barrier of the catalytic reduction reaction of 4-nitrophenolate(aq) substantially to enhance the catalytic performances of Au@mSiO$_2$ NRs largely.

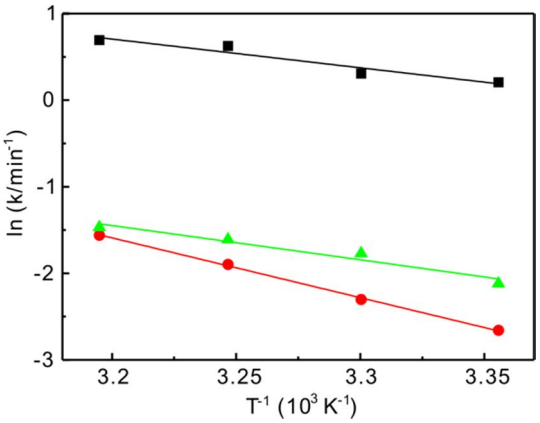

Figure 1-6. Arrhenius plots of rate constants for the reduction of 4-nitrophenolat(aq) catalyzed by 13 pM of (squares) Au@CTAB NRs, (circles) Au@mSiO$_2$ NRs, and (triangles) irradiated Au@mSiO$_2$ NRs in the presence of NaBH$_4$.

Table 1-1. Rate constants, induction times, frequency factors, activation energies, and activation entropies for the catalytic degradation of 4-nitrophenol via nanocatalysts in the presence of NaBH$_4$.

Nanocatalyst	Concentration of nanocatalyst pM (ng L^{-1})	Rate constant at 25 °C min^{-1}	Induction time at 25 °C min	Frequency factor min^{-1}	Activation energy kcal mol^{-1}	Entropy of activation cal mol^{-1} K^{-1}
Au@mSiO$_2$	9 (1.8)	0.059	20.0	1.47×10^8	12.9	-23.2
Au@mSiO$_2$	13 (2.6)	0.086	16.4	2.43×10^8	12.9	-22.2
Au@mSiO$_2$	17 (3.3)	0.105	10.1	8.74×10^8	13.5	-19.7
Au@CTAB	13 (2.6)	1.232	1.6	7.57×10^4	6.5	-38.2
Irr. Au@mSiO$_2$	13 (2.6)	0.121	6.9	3.33×10^4	7.4	-39.4

Table 1 gives a comparison of rate constants, induction times, frequency factors, activation energies, and activation entropies when the reduction of 4-nitrophenolate(aq) is

catalyzed by three different gold nanocatalysts. As seen in Table 1, Au@CTAB NRs have a better catalytic activity than silica-coated gold nanorods catalysts at the first cycle of catalytic experiment, suggesting that the access of reactants to the surface sites of core gold nanorods is disturbed by silica coverage. This implies that the deposition of mesoporous silica onto Au@CTAB NRs raises the barrier of the reaction. Table 1 shows that the frequency factor of the catalytic reduction of 4-nitrophenolate(aq) via irradiated Au@mSiO_2 NRs is much smaller than that via Au@mSiO_2 NRs, suggesting that the large increase of the catalytic rate constant by the light irradiation of Au@mSiO_2 NRs is due to decrease in the activation energy of the reduction reaction. The detailed mechanism of light treatment for the enhancement of the catalytic performances of Au@mSiO_2 NRs will be discussed later. Eyring plots [35] using temperature-dependent rate constants have revealed that the entropies of activation for catalytic reactions via Au@CTAB NRs and irradiated Au@mSiO_2 NRs are similar to each other and have large negative values whereas the entropy of activation for the catalytic reaction via Au@mSiO_2 NRs has a relatively smaller negative value. This also indicates that the catalytic mechanism of irradiated Au@mSiO_2 NRs is similar to that of Au@CTAB NRs in spite that Au NRs are surrounded by silica shells.

The dependence of catalytic performances on the concentration of Au@mSiO_2 NRs in the reduction of 4-nitrophenol in the presence of $NaBH_4$ has been reported in Table 1 and Fig. S5 in Supporting Information. The rate constant increases almost linearly with the concentration of the nanocatalyst. On the other hand, the frequency factor also increases linearly with the catalyst concentration whereas the activation energy remains almost invariant regardless of the concentration. This suggests that the rate constant increases as the frequency factor, which depends on the total surface area of the nanocatalyst, increases with the concentration, and that the catalytic mechanism are the same regardless of the dosage of the nanocatalyst.

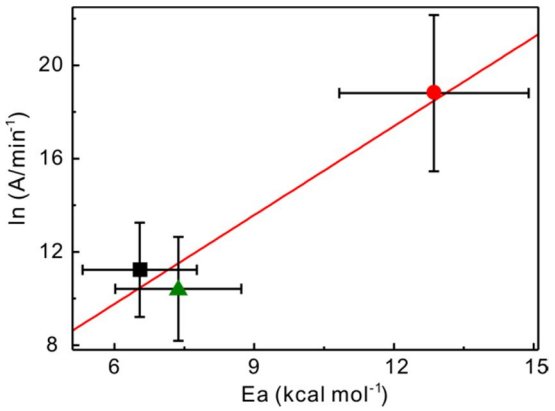

Figure 1-7. The compensation law plot of the activation energies and the frequency factors obtained from the slopes and the intercepts, respectively, of the Arrhenius plots of Fig. 6.

Fig. 7 is a plot of frequency factors versus activation energies for the reduction of 4-nitrophenolate catalyzed with three different catalysts used. Fig. 7 shows the existence of a good compensation relation in the catalytic systems of gold nanorods. The following empirical linear relationship has been found to hold between the frequency factor (A) and the activation energy (E_a): $\ln A = \alpha + E_a / (RT_\theta)$ where α is a constant and T_θ is called the fictitious isokinetic temperature, at which the catalytic rates of all the nanocatalysts become equal [36,37]. In our experiments, T_θ has been found to be 396 K. Fig. 7 suggests that both nanocatalysts of Au@CTAB NRs and irradiated Au@mSiO_2 NRs have a smaller concentration of active sites where the reaction requires small Ea, whereas the nanocatalyst of Au@mSiO_2 NRs has a large concentration of active sites that have high Ea for the same catalytic reaction. This implies that light treatment has converted the catalytic mechanism of silica-coated gold nanorods into that of uncoated gold nanorods, enhancing the catalytic performances of Au@mSiO_2 NRs on a large scale.

1.4.4. Induction Time

As mentioned earlier, Fig. 5 demonstrates that a certain period of time was required for reactants to adsorb onto the surfaces of core gold nanorods before the catalytic reaction was initiated. This period is well known as the induction time (t_0) [9,10,31,38-42]; it has been attributed to a slow diffusion of reactants onto the catalytic surfaces [40] or a dynamic restructuring of the surface of the nanocatalysts due to adsorbate-surface interactions [42,43]. Fig. S6 in Supporting Information shows that in our experimental conditions, the induction time with Au@mSiO$_2$ NRs is much longer than that with Au@CTAB NRs. The reduction reaction of 4-nitrophenolate via catalysts has been explained based on the Langmuir-Hinshelwood mechanism that the catalytic reaction takes place when both species of electron donor BH_4^- and electron acceptor 4-nitrophenolate adsorb onto the catalyst surfaces [9]. Thus, the induction period with Au@mSiO$_2$ NRs is observed to be much larger than that with Au@CTAB NRs because it takes a longer time to diffuse through the mesoporous silica shell. Furthermore, the induction time with Au@mSiO$_2$ NRs decreases sharply with increasing temperature whereas that with Au@CTAB NRs changes hardly. This suggests that the penetration of reactants through the silica shell requires going through a considerable energy barrier. Fig. S6 reveals that the light treatment of Au@mSiO$_2$ NRs reduces the induction time substantially while it hardly diminishes the activation energy of the induction process. Thus, we suggests that light treatment reduces the induction time mainly by reducing the surface restructuring time of gold nanorods induced by adsorbed reactants [42,43] while it does hardly reduces the diffusion time of reactants through silica shell [40]. These results imply that light treatment does not deteriorate the protection of gold nanorods by silica shells while it decreases the induction time largely and enhances the catalytic rate constant greatly.

1.4.5. Catalytic Reusability

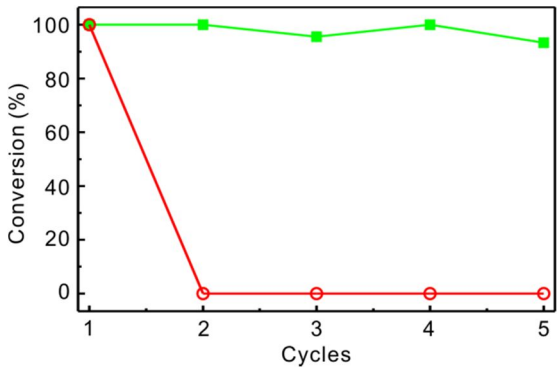

Figure 1-8. Conversion of 4-nitrophenol measured at 35 min in five successive catalytic reduction cycles via 9 pM of (squares) irradiated Au@mSiO$_2$ NRs and (circles) Au@CTAB NRs in the presence of NaBH$_4$.

The reusable ability of the nanocatalysts of Au@CTAB NRs and irradiated Au@mSiO$_2$ NRs has been measured by repeating catalytic experiments. For these studies, the concentrations of nanocatalysts as well as other conditions were held constant. Catalysis recycle experiments were performed five times to prove the catalytic stability of nanocatalyts. Both nanocatalysts were separated by centrifugation and reused for consecutive catalysis reactions. The reusability of nanocatalysts shown in Fig. 8 displays that Au@CTAB NRs do not have catalytic efficiency at all from the second cycle, whereas irradiated Au@mSiO$_2$ NRs maintain similar catalytic performance so that the catalytic conversion efficiency is still as high as 91% in the fifth cycle. These results also suggest that the encapsulation effect of mesoporous silica, which enhances the stability of nanocatalysts by preventing the aggregation and dissolution of gold nanorods, remains intact in irradiated Au@mSiO$_2$ NRs regardless of light treatment.

1.4.6. Effect of Light Treatment on Catalytic Performances

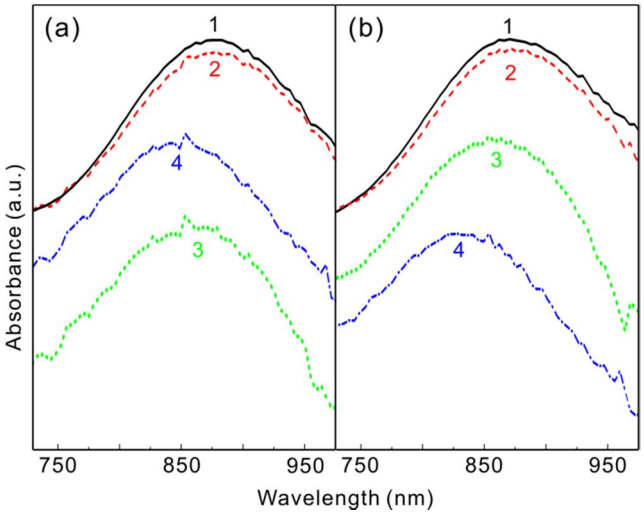

Fig. 9. Surface-plasmon resonance spectra of the nanocatalysts of (a) Au@mSiO$_2$ NRs and (b) irradiated Au@mSiO$_2$ NRsafter mixing (1) nothing, (2) 4NP, (3) 4NP and NaBH$_4$ at 0 min, and (4) 4NP and NaBH$_4$ at 30 min.

As already discussed in the section 1.4.2, the λ_{max} of irradiated Au@mSiO$_2$ NRs (875 nm) is shifted to the blue by 5 nm from that of Au@mSiO$_2$ NRs (880 nm). This suggests that the aspect ratios of mesoporous silica-coated gold nanorods have been decreased very slightly by the photothermal annealing effect of gold nanorods during light irradiation. On the other hand, it is well-known that the metal nanoparticles catalyze the reduction reaction of 4NP in the presence of NaBH$_4$ by facilitating electron relays from the donor BH_4^- to acceptor 4NP to overcome the kinetic barrier [34]; the rate of electron transfer on the Au NR surface could be influenced by the following two-step mechanism [12] :

$$BH_4^- \rightarrow BH_3 + H^* \text{ (on Au NR surface)} + e^- \quad (1)$$

$$6\ H^* \text{ (on Au NR surface)} + \text{4-nitrophenol} \rightarrow \text{4-aminophenol} + 2H_2O \quad (2)$$

The nucleophile BH_4^- can donate electrons to gold nanocatalysts, and the electrophile 4NP can capture electrons from the gold nanocatalysts. Therefore, the reduction of 4NP takes place on the surface of the gold nanocatalysts by the reaction of adsorbed 4NP with surface-hydrogen species [9] and gold nanocatalysts serve as electron relays. We have monitored changes in the surface-plasmon resonance spectra of the nanocatalysts to understand differences in the catalytic mechanisms of Au@mSiO_2 NRs and irradiated Au@mSiO_2 NRs. Because the movement of electrons on the surfaces of gold nanorods is directly related to surface-plasmon resonances (SPR), the monitoring of SPR band positions can provide information on the quantity of electrons on the metallic surface during a catalytic reaction [12]. Fig. 9 shows that the SPR band did not shift at all after the addition of 4-nitrophenol to the nanocatalyst of either Au@mSiO_2 NRs or irradiated Au@mSiO_2 NRs. However, as soon as $NaBH_4$(aq) was added, the SPR bands of Au@mSiO_2 NRs and irradiated Au@mSiO_2 NRs shifted to the blue by 12 and 17 nm, respectively. These SPR band shifts right after the addition of $NaBH_4$(aq) strongly support the fact that the silica shells have the mesoporous structure, because immediate SPR band shifts imply that BH_4^- reactants have reached rapidly onto core surfaces through the pores of the silica shells. The blue shift of irradiated Au@mSiO_2 NRs, which is much larger than that of non-irradiated Au@mSiO_2 NRs, indicates that more electrons exist on the core surface of irradiated Au@mSiO_2 NRs [12]. It is reported that a nanocatalyst having a higher electron density catalyzes the conversion of 4-nitrophenol more rapidly [12]. Therefore, it is suggested that light treatment has induced the metallic-surface restructuring of Au@mSiO_2 NRs that facilitates electron transfer form BH_4^- to the metallic surface during the catalytic reaction. This can also partially explain the increased rate of the catalytic reaction via irradiated Au@mSiO_2 NRs. In addition, at 30 min after adding $NaBH_4$ (aq), the SPR band shifts of Au@mSiO_2 NRs and irradiated Au@mSiO_2 NRs become

30 and 43 nm, respectively, to the blue, compared SPR in the absence of $NaBH_4$. These results also illustrate that although excess $NaBH_4$ has been added in the catalytic reaction mixture to ensure pseudo-first-order kinetic conditions, BH_4^- species adsorbs onto irradiated Au@$mSiO_2$ NRs more readily than onto non-irradiated Au@$mSiO_2$. Taking everything into consideration, we could say that the surface atom restructuring, resulting from photothermal annealing during irradiation, renders the metallic surface easy to adsorb reactants and to facilitate electron relays from electron-donor BH_4^- to electron-acceptor 4-nitrophenol. This makes irradiated Au@$mSiO_2$ NRs catalytically much more active than non-irradiated Au@$mSiO_2$ NRs, lowering the kinetic barrier that depends on the structure of catalytic active sites [38].

We have also taken into consideration of the role of the CTAB surfactant in the formation of the mesoporous silica shell to explain the enhanced catalytic performances of the irradiated nanocatalyst. Negatively charged silica sols are reported to bind to positively charged cetyltrimethylammonium ions adsorbed on the surface of Au NRs via electrostatic interactions [29,44]. Thus, CTAB surfactants strongly localized on individual Au NR surfaces act as templates, promoting mesoporous-shell deposition directly onto the NR surfaces [16]. Extensive decrease in the induction time of Au@$mSiO_2$ NRs via light treatment could be explained by the suggestion that a large amount of remnant CTAB resulting from the formation of mesoporous silica shells desorbs from mesoporous silica shells during irradiation to be soluble in the solvent. As already shown, the average aspect ratio of Au@$mSiO_2$ has decreased slightly by irradiation, demonstrating that surface reconstruction has taken place during light treatment. The thermal-induced melting of gold NRs starts at their surfaces [45] and surface atoms are known to get mobility at the Hüttig temperature ($0.3T_{melting}$) [46]. Thus, the movement of atoms on the surfaces weakens the bond strength

between CTAB and gold surfaces and renders the surfaces to have strong interactions with reactants, making the adsorption of reactants on catalytic metal surfaces easy. Thus, it is suggested that light treatment reduces the induction time largely because it can make reactants penetrate through CTAB-reduced silica shells rapidly and adsorb onto restructured metallic surfaces easily.

1.5. Conclusions

CTAB-stabilized gold nanorods (Au@CTAB NRs) with an average diameter of 17.5 nm and a typical aspect ratio of 4 have been encapsulated by mesoporous silica shells having a uniform thickness of 20 nm to form silica-coated gold nanorods (Au@$mSiO_2$ NRs), which have been further treated by being irradiated with a Xe lamp for 2 h to produce irradiated Au@$mSiO_2$ NRs. The catalytic studies of three different nanocatalysts of Au@CTAB NRs, Au@$mSiO_2$ NRs, and irradiated Au@$mSiO_2$ NRs by monitoring the time-dependent reduction of 4-nitrophenol in the presence of $NaBH_4$ have indicated that light treatment enhances the catalytic performances of Au@$mSiO_2$ NRs on a large scale without deteriorating the encapsulation effect of mesoporous silica that enhances the stability and reusability of the nanocatalyst by preventing the aggregation and dissolution of gold nanorods. Irradiation has increased the catalytic rate constant largely and reduced the activation energy and the induction time of the catalytic reaction considerably; surface atom restructuring by photothermal annealing during irradiation has rendered the metallic surface to adsorb reactants readily and to promote rapid electron relays from BH_4^- to 4-nitrophenol, lowering the kinetic barrier of the catalytic reaction substantially. Thus, it is suggested that post light treatment introduced here is a simple and green method applicable widely in the field of nanocatalysis.

1.6. Acknowledgments

This work was supported by research grants through the National Research Foundation of Korea (NRF) funded by the Korea government (2012-006345 and 2011-0028981). D.J.J. is also thankful to the SRC program of NRF (2007-0056095).

1.7. Supporting Information

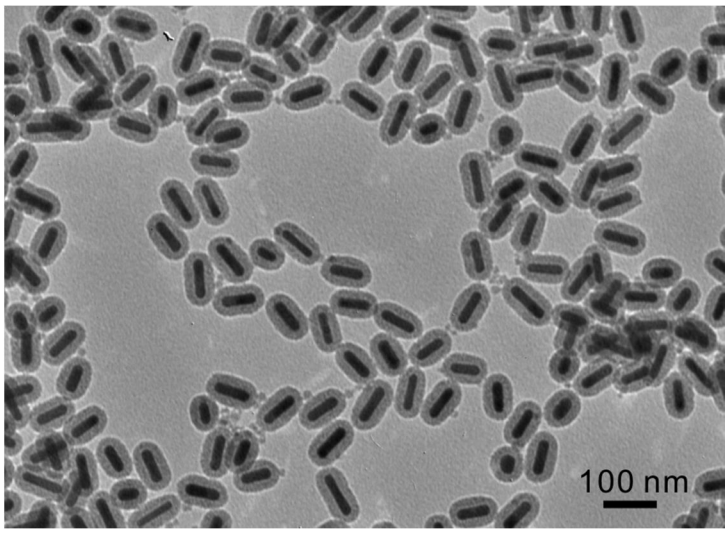

Fig. S1. Low-magnification TEM image of Au@mSiO$_2$ NRs.

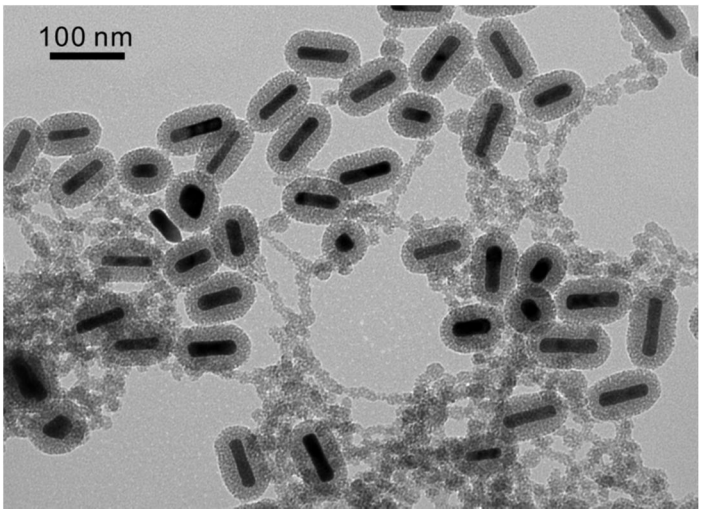

Fig. S2. TEM image of Au@mSiO$_2$ NRs prepared at a high concentration of CTAB.

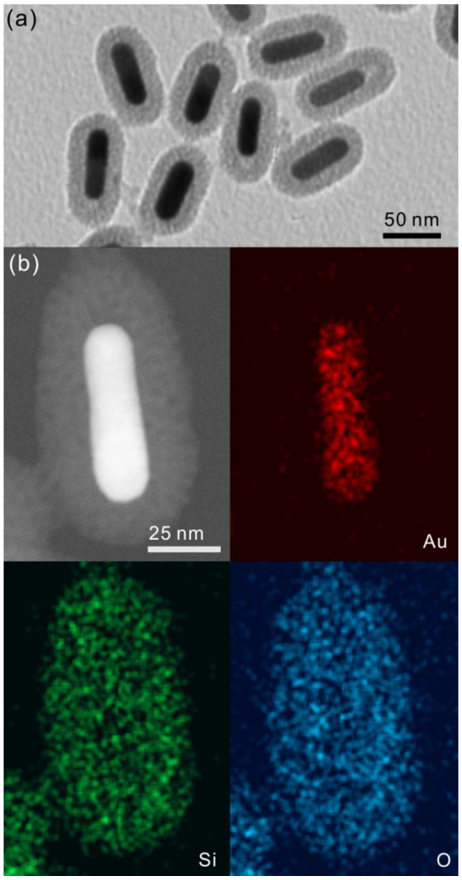

Fig. S3. (a) TEM image of irradiated Au@mSiO$_2$ NRs and (b) STEM image and EDX elemental maps of a irradiated Au@mSiO$_2$ NR.

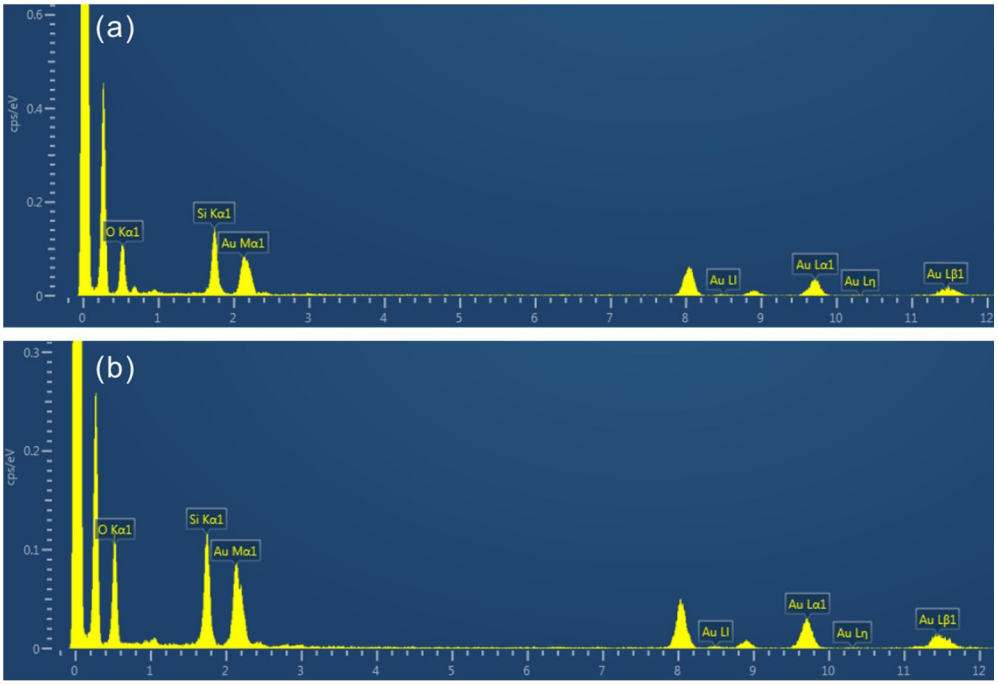

Fig. S4. EDX spectra of (a) Au@mSiO$_2$ NRs and (b) irradiated Au@mSiO$_2$ NRs, showing the presence of Si, O, and Au.

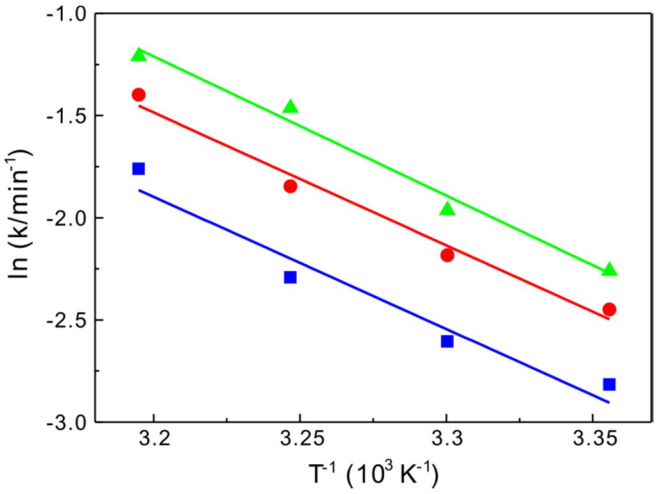

Fig. S5. Arrhenius plots of rate constants for the reduction of 4-nitrophenol(aq) catalyzed by (squares) 9 pM, (circles) 13 pM, and (triangles) 17 pM of Au@mSiO$_2$ NRs in the presence of $NaBH_4$.

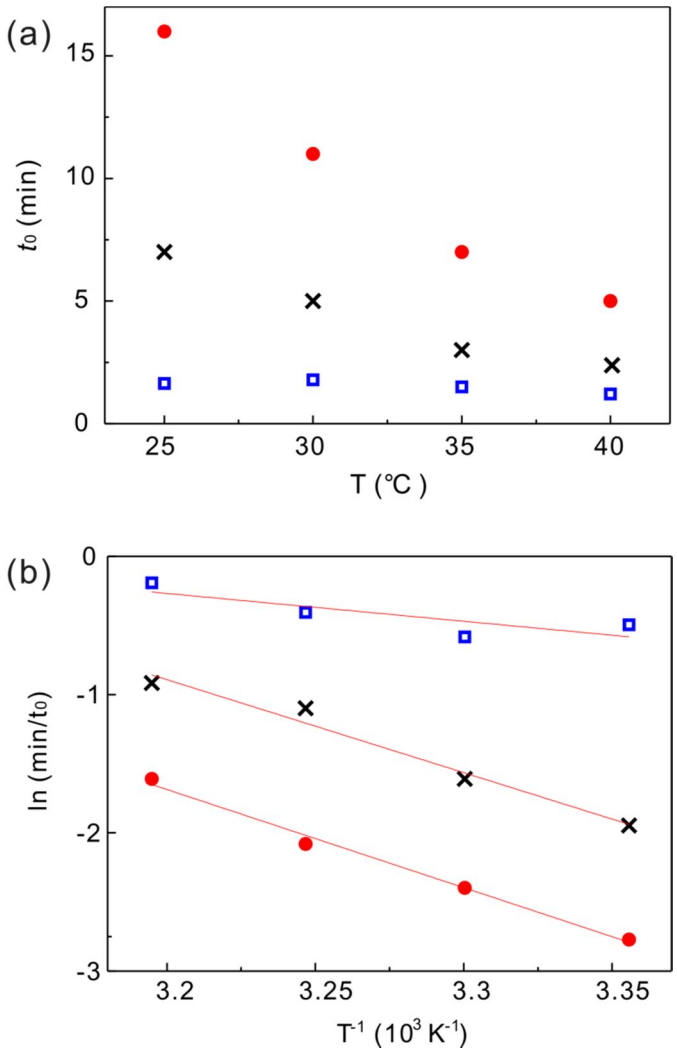

Fig. S6. (a) Temperature-dependent induction times and (b) Arrhenius plots of inversed induction times for the reduction of 4-nitrophenol catalyzed by 13 pM of (circles) Au@mSiO$_2$ NRs, (crosses) irradiated Au@mSiO$_2$ NRs, and (squares) Au@CTAB NRs in the presence of $NaBH_4$. Ea values are estimated as 14.1, 13.4, and 4.0 kcal mol^{-1} from the Arrhenius plots of Au@mSiO$_2$ NRs, irradiated Au@mSiO$_2$ NRs, and Au@CTAB NRs.

1.8. References

[1] Y. Kim, D.-J. Jang, Chem. Commun. 49 (2013) 8940-8942.

[2] J.-Y. Kim, D. Lee, H.J. Kim, I. Lim, W.I. Lee, D.-J. Jang, Mater. Chem. A 1 (2013) 5982-5988.

[3] M. Salerno, J.R. Krenn, B. Lamprecht, G. Schider, H. Ditlbacher, N. Felidj, A. Leitner, F.R. Aussenegg, Opto-Electron. Rev. 10 (2002) 217-224.

[4] R.R. Arvizo, S. Bhattacharyya, R.A. Kudgus, K. Giri, R. Bhattacharya, P. Mukherjee, Chem. Soc. Rev. 41 (2012) 2943–2970.

[5] S. Kundu, S. Lau, H. Liang, J. Phys. Chem. C 113 (2009) 5150-5156.

[6] P.G.N. Merten, P. Vandezande, X. Ye, H. Poelman, I.F.J. Vankelecom, D.E. De Vos, Appl. Catal. A 355 (2009) 176-183.

[7] Y. Zhang, X. Cui, F. Shi, Y. Deng, Chem. Rev. 112 (2012) 2467-2505.

[8] L.-F. Gutiérrez, S. Hamoudi, K. Belkacemi, Catalysts 1 (2011) 97-154.

[9] S. Wunder, Y. Lu, M. Albercht, M. Ballauff, ACS Catal. 1 (2011) 908-916.

[10] J. Zeng, Q. Zhang, J. Chen, Y. Xia, Nano Lett. 10 (2010) 30-35.

[11] X. Bai, Y. Gao, H. Liu, L. Zheng, J. Phys. Chem. C 113 (2009) 17730-17736.

[12] M. Eo, J. Baek, H.D. Song, S. Lee, J. Yi, Chem. Commun. 49 (2013) 5204-5206.

[13] Z. Zhang, J. Wang, C. Chen, Theranostics 3 (2013) 223-238.

[14] J. Pérez-Juste, I. Pastoriza-Santos, L.M. Liz-Marzán, P. Mulvaney, Coord. Chem. Rev. 249 (2005) 1870-1901.

[15] C. Wu, Q. Xu, Langmuir 25 (2009) 9441-9446.

[16] I. Gorelikov, N. Matsuura, Nano Lett. 8 (2008) 369-373.

[17] J. Chen, R. Zhang, L. Han, B. Tu, D. Zhao, Nano Res. (2013) DOI: 10.1007/s12274-013-0363-1.

[18] J.C. Park, H. Song, Nano Res. 4 (2011) 33-49.

[19] I. Lee, J. B. Joo, Y. Yin, F. Zaera, Angew. Chem. Int. Ed. 50 (2011) 10208-10211.

[20] M. Kim, K. Sohn, H.B. Na, T. Hyeon, Nano Lett. 2 (2002) 1383-1387.

[21] S.H. Joo, J.Y. Park, C. Tsung, Y. Yamada, P. Yang, G.A. Somorjai, Nat. Mater. 8 (2009) 126-131.

[22] Y. Chen, H. Chen, D. Zeng, Y. Tian, F. Chen, J. Feng, J. Shi, ACS Nano 4 (2010) 6001-

6013.
[23] C. Gautier, A.L. Cunningham, L. Si-Ahmed, G. Robert, T. Bürg, Gold Bull. 43 (2010) 94-104.
[24] Z. Zhang, L. Wang, J. Wang, X. Jiang, X. Li, Z. Hu, Y. Ji, X. Wu, C. Chen, Adv. Mater. 24 (2012) 1349-1493.
[25] W. Annan, P. Qing, L. Yadong, Chem. Mater. 23 (2011) 3217-3222.
[26] M. A. Mahmoud, F. Saria, M. A. El-Sayed, Nano Lett. 10 (2010) 3764-3769.
[27] C. J. Orendorff, C. J. Murphy, J. Phys. Chem. B 110 (2006) 3990-3994.
[28] Q. Zhan, J. Qian, X. Li. S. He, Nanotechnology 21 (2010) 055704.
[29] C.-C. Huang, C.-H. Huang, I.-T. Kuo, L.-K. Chau, T.-S. Yang, Colloids Surf. A 409 (2012) 61-68.
[30] L.M. Liz-Marzán, M.Giersig, P. Mulvaney, Langmuir 12 (1996) 4329-4335.
[31] S. Panigrahi, S. Basu, S. Praharaj, S. Pande, S. Jana, A. Pal, S.K. Ghosh, T. Pal, J. Phys. Chem. C 111 (2007) 4596-4605.
[32] T. Vincent, E. Guibal, Langmuir 19 (2003) 8475-8483.
[33] S.K. Srivastava, R. Yamada, C. Ogino, A. Kondo, Nanoscale Res. Lett. 8 (2013) 70.
[34] A. Gangula, R. Podila, R. M, L. Karanam, C. Janardhana, A.M. Rao, Langmuir 27 (2011) 15268-15274.
[35] K.D. Zimmer, R. Shoemaker, R.R. Ruminski, Inorg. Chim. Acta 359 (2006) 1478-1484.
[36] J.-A. Kwak, D.K. Lee, D.-J. Jang, Appl. Catal. B: Environ. 142-143 (2013) 323-328.
[37] T. Bligaard, K. Honkala, A. Logadottir, J.K. Nørskov, S. Dahl, C.J.H. Jacobsen, J. Phys. Chem. B 107 (2003) 9325-9331.
[38] M.A. Mahmoud, M.A. El-Sayed, Nano Lett. 11 (2011) 946-953.
[39] J. Lee, K. Han, D.-J. Jang, Appl. Catal. A: Gen. 469 (2014) 380-386.
[40] K. Kuroda, T. Ishida, M. Haruta, J. Mol. Catal. A: Chem. 298 (2009) 7-11.
[41] H. Yamamoto, H. Yano, H. Kouchi, Y. Obora, R. Arakawa, H. Kawasaki, Nanoscale 4 (2012) 4148-4154.
[42] P. Hervés, M. Pérez-Lorenzo, L.M. Liz-Marzán, J. Dzubiella, Y. Lubc, M. Ballauff, Chem. Soc. Rev. 41 (2012) 5577-5587.
[43] X. Zhou, W. Xu, G. Liu, D. Panda, P. Chen, J. Am. Chem. Soc. 132 (2010) 138-146.
[44] R.I. Nooney, D. Thirunavukkarasu, Y. Chen, R. Josephs, A.E. Ostafin, Langmuir 19

(2003) 7628-7637.
[45] H. Petrova, J.P. Juste, I. Pastoriza-Santos, G.V. Hartland, L.M. Liz-Marzan, P. Mulvaney, Phys. Chem. Chem. Phys. 8 (2006) 814-821.
[46] J.A. Moulijn; A.E. van Diepen, F. Kaptijn, Appl. Catal. A 212 (2001) 3-16.

Chapter 2. Laser-Induced Welding of Self-Assembled Gold Nanorods to Fabricate Au@SiO_2 Core-Shell Nanowires

2.1. Abstract

Au@SiO_2 core-shell nanowires have been successfully fabricated by irradiating infrared nanosecond pulses to linearly self-assembled and silica-coated gold nanorods. Gold nanorods have been self-assembled linearly by adding isopropanol in the absence of any assembling agents to form gold nanochains. The end-to-end assembled gold nanorods then have been directly encapsulated with uniform silica shells having tunable thickness to produce silica-coated gold nanochains. The irradiation of the nanostructures loaded on a TEM grid for 5 min with nanosecond laser pulses of 1064 nm at fluence of 0.38 mJ/cm^2 has produced Au@SiO_2 core-shell nanowires. This is a novel and straightforward synthetic approach for the production of silica-coated gold nanowires having strong near-infrared absorption, high stability, and easily functionalizable surface.

2.2. Introduction

The design and fabrication of nanostructured materials with functional spectroscopic, electronic, and chemical properties have been widely explored because of their potential applications in catalysis, optoelectronics, and transistors.[1-4] Particularly, noble-metal nanoparticles have attracted much attention in the field of catalysis,[5-7] optoelectronics,[8] and biological and chemical sensing[9] especially due to their tunable optical properties originating from their surface-plasmon resonance (SPR); it is the collective oscillation of conducting electrons on a metallic surface and can be tuned by controlling the sizes, shapes, and compositions of nanoparticles.[10] There is considerable attention to assemble these nanoparticles as building blocks into an ordered structures and further into functional devices through a bottom-up approach because it offers the promising properties that are absent in the corresponding individual nanoparticles.[11-13]

Gold nanorods (NRs) exhibit rich SPR-derived properties, which have made them useful for many interesting applications such as optical and optoelectronic devices,[14,15] sensors,[16] and biomedical technologies.[17] Gold NRs possess two distinctive, transverse and longitudinal, SPR modes, the latter one of which exhibits a strong peak tunable from the visible to the near-infrared region with increasing aspect ratios. Gold NRs also have a unique property that converts light efficiently into heat through so-called a photothermal effect.[18,19] Increasing attention has been paid to the assembly of gold NRs in solutions, and a variety of techniques have been developed to induce the assembly of gold NRs in an either end-to-end or side-by-side manner in solutions by functionalizing the surface of gold NRs preferentially; the assembly has been reported to occur through electrostatic interactions,[20-22] hydrogen bonding,[23] covalent bonding,[24,25] or biorecognition

interaction.[12,26,27] Recently, spontaneous self-linking has been obtained in the absence of any assembling agents by diluting the concentration of cetyltrimethylammonium bromide (CTAB) in gold NR colloidal solutions.[28,29] As gold NRs are assembled especially in an end-to-end orientation, a new hybridized plasmon mode appears in the longer-wavelength region of the gradually disappearing longitudinal SPR mode due to the coupling of surface-plasmon resonances between the nanorods.[23] These plasmon coupling properties of linearly assembled nanostructures give rise to extend the application of gold NRs to areas such as optoelectronics,[30] surface-enhanced Raman scattering and sensing,[31,32] and near infrared-resonant biomedical fields.[33-36] These assembly approaches, often induced by organic molecules as an assembling agent, require organic environment such as an acetonitrile-water (4:1 v/v) mixture because the solubility of the assembling agent is low in water.[20,23-25,37] Thus, the assembled structures are often structurally unstable during storage and purification, being aggregated irreversibly and losing their desirable optical properties.[38] Although significant progresses have been made in the self-assembly of gold NRs, the *in situ* stabilization methods of as-prepared assemblies in solutions have to be developed to utilize the assemblies for a further process, which is important in the fabrication of functional nanostructures. The encapsulation of assembled gold nanoparticles within a silica or polymer shell to stabilize products has been demonstrated.[13,38-42] However, a direct encapsulation method of anisotropically assembled gold NRs with uniform shells still remains to be designed since direct shell coating onto CTAB-stabilized gold NRs, via a sol-gel process as an example, requires sensitive conditions.

In this paper, we report a straightforward approach to fabricate a silica-coated gold nanowire via self-assembly of gold NRs to form a gold nanochain, followed by encapsulation of the nanochain in a uniform silica shell and nanowelding of the silica-coated nanochain by

laser irradiation to produce a Au@SiO_2 core-shell nanowire (Figure 1). We have observed that gold nanorods can be assembled spontaneously in an end-to-end orientation upon addition of isopropanol without using any assembling agents and that direct *in situ* coating with silica has made the assembled gold nanochain stable in ethanol over a year. The simple irradiation of the silica-coated gold nanochain by nanosecond laser pulses of 1064 nm for 5 min has been found to yield a Au@SiO_2 core-shell nanowire.

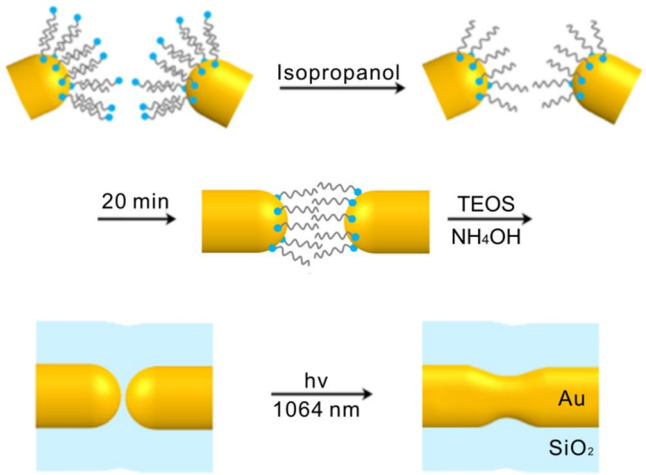

Figure 1. Schematic for the fabrication of a silica-coated gold nanowire.

2.3. Experimental Section

Ascorbic acid(s, 99.9%), CTAB(s, 96%), $HAuCl_4 \cdot 3H_2O$(s, 99.9%), isopropanol(*l*), ethanol(*l*), $AgNO_3$(s, ≥99%), $NaBH_4$(s, 96%), ammonium hydroxide(*aq*, 33%), and tetraethyl orthosilane (TEOS, *l*, ≥99%) were used as purchased from Sigma-Aldrich. Ultrapure deionized water (>17 MΩ cm) was obtained using a Millipore Milli-Q system.

CTAB-stabilized gold nanorods dispersed in water, having an average length of 42.5 nm with a typical aspect ratio of 4.2 and the absorption maximum of longitudinal surface-plasmon resonances at 830 nm, were synthesized according to a reported seed-mediated and CTAB-assisted method.[43] The aqueous colloidal solution of as-synthesized gold NRs was centrifuged at 8500 rpm for 8 min to remove excess CTAB, and the precipitates were redispersed in 16 mL of water. The centrifugation and dispersion processes were repeated. The concentration of gold NRs in the finally purified colloidal solution was calculated to be 1.0 nM based on their extinction coefficient[44] while the concentration of CTAB in the colloidal solution was estimated to be 0.12 mM.

The end-to-end self-assembly of gold nanorods was obtained by adding 1.0 mL of the above-prepared gold NR colloidal solution into 5.0 mL of isopropanol under continuous stirring. It is important to note that the gold NR colloid had been stored at least for a month prior to the addition of isopropanol. After being stirred for 20 min, gold nanochains, which were linearly self-assembled gold NRs, were subsequently coated with silica by following a reported method[45] with some modifications. The resulting assembled colloidal solution was slowly added with a specific volume (0.50 mL if not specified otherwise) of 3.8% ammonium hydroxide in isopropanol under vigorous stirring to produce silica-coated gold nanochains. Then, 20 μL of 20% TEOS in isopropanol was added immediately and stirred for

2 h at room temperature. The mixture was left undisturbed and aged for 20 h in a refrigerator. The resultant colloid was centrifuged at 3500 rpm for 25 min, the supernatant was washed away 3 times with ethanol, and the final products were stored in ethanol.

1.2 μL of the colloid containing silica-coated gold nanochains in ethanol was loaded onto a TEM grid and irradiated to weld gold nanorods for the fabrication of silica-coated gold nanowires by using 0.74 mJ nanosecond laser pulses of 1064 nm having a duration of 6 ns from a Quantel Brilliant Q-switched Nd:YAG laser run at 10 Hz. The spot diameter of the irradiation laser beam was 3 mm, and the laser power was measured by using an energy detector (Gentec-EO, UP 19K-15S-VH-DO) connected to a power and energy monitor (Gentec-EO, SOLO PE). While transmission electron microscopic (TEM) images were obtained with a Hitachi H-7600 microscope, high-resolution TEM (HRTEM) and scanning TEM (STEM) images and energy-dispersive X-ray (EDX) elemental maps and profiles were measured by using a JEOL JEM-2100F microscope. Absorption spectral changes of surface-plasmon resonances with the self-assembly of gold nanorods were monitored by measuring absorption spectra at scheduled intervals using a UV/vis spectrophotometer (Scinco, S-3000).

2.4. Results and Discussion

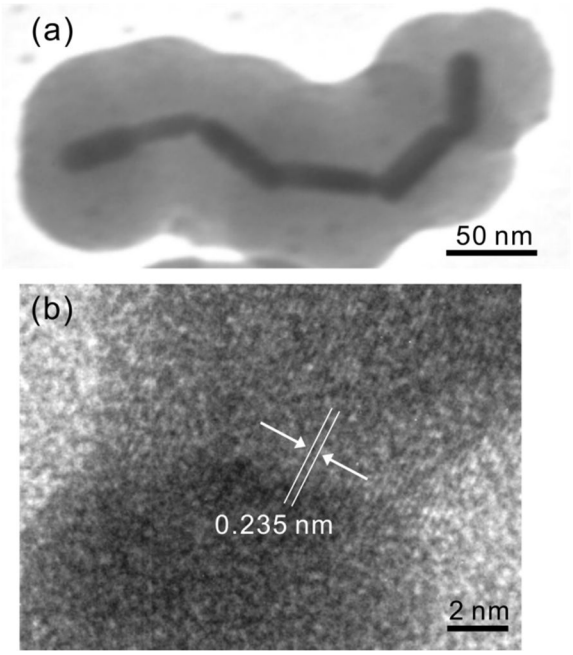

Figure 2. (a) TEM image and (b) HRTEM image of a gold nanowire. Nanowelding of silica-coated gold nanorods on a TEM grid has been carried out by 6 ns laser pulses of 1064 nm for 5 min at fluence of 0.38 mJ cm^{-2}.

Figure 2a shows that linearly assembled gold NRs in a silica-coated gold nanochain loaded on a TEM grid have been welded together by nanosecond laser pulses of 1064 nm to have nanocontact, producing a Au@SiO_2 core-shell nanowire. Although neighboring gold NRs in a silica-coated gold nanochain did not have ohmic contact on each other, they have been well nanojoined together by laser irradiation to form a silica-coated gold nanowire. The HRTEM image of Figure 2b reveals the detailed crystalline structure at a welded nanojunction of a Au@SiO_2 core-shell nanowire; two gold NRs at the conjunction are well fused together in a single phase to have ohmic contact. An interlayer spacing of 0.235 nm observed in the core region of a Au@SiO_2 nanowire agrees well with the literature spacing

value of 0.2355 nm between the (111) lattice planes of the fcc Au crystal (JCPDS 04-0784).

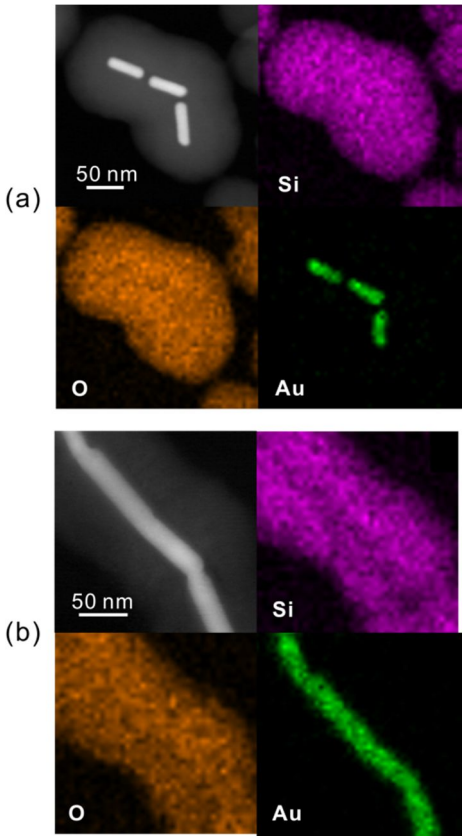

Figure 3. STEM images and corresponding EDX elemental maps of (a) a silica-coated gold nanochain and (b) a silica-coated gold nanowire.

The STEM image of Figure 3a reveals that gold NRs in a silica-coated gold nanochain have their original nanorod shapes without being connected via metallic bonds; they are separated from each other by a distance of 8 nm, which has been maintained by linearly assembling CTAB molecules. However, the STEM image of Figure 3b indicates that gold NRs in a silica-coated gold nanowire have been fused together with showing ohmic nanocontact. The EDX elemental maps of Figure 3 show the detailed structures of the silica-coated gold nanostructures. Silica consisting of Si and O atoms encapsulates both the gold

nanochain and the gold nanowire well with uniform shell thickness. The EDX elemental maps also display that irradiation with nanosecond pulses of 1064 nm for a short time of 5 min has transformed a silica-coated gold nanochain into a Au@SiO_2 core-shell nanowire indeed.

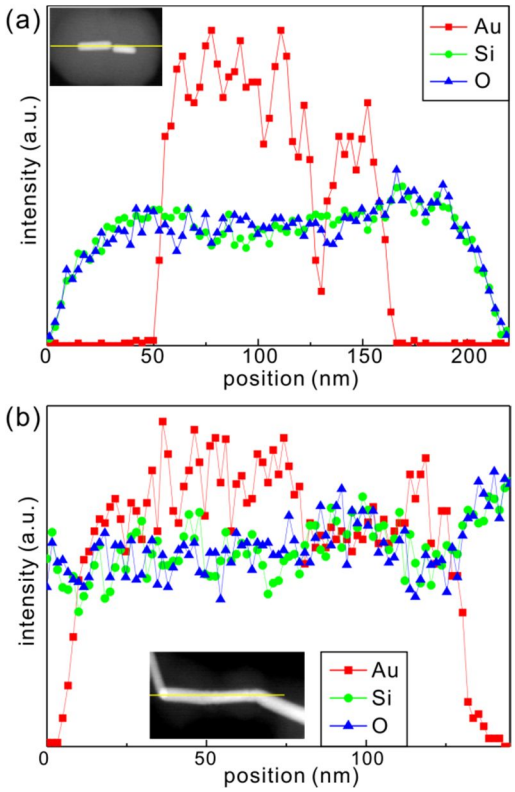

Figure 4. Area-normalized EDX elemental profiles of (a) a silica-silica coated gold nanochain and (b) a silica-coated gold nanowire scanned along the lines in the STEM images of the insets.

The EDX elemental profiles of a silica-coated gold nanochain and a Au@SiO_2 core-shell nanowire scanned along the indicated solid lines of the insetted STEM images in Figure 4 also show that the gold nanostructures are present at the cores of the nanocomposites while silica consisting of silicon and oxygen atoms surrounds the gold assemblies. The detailed EDX analysis of Figure 4a indicates that gold nanochain structure is capped by silica with showing discontinuity at a position of 130 nm. However, Figure 4b clearly shows that the

gold atoms are continuously present without showing any discontinuity at the conjunction positions. The continuous intensity profile of gold in the longitudinal direction of the welded gold nanowire also reveals that the contacting surfaces between the initial gold nanorods have been fused by laser irradiation to be welded together.

It has been already reported[46] that a Au@CdS core-shell nanowire can be obtained by exciting the surface-plasmon resonances of gold nanospheres, priorly connected by dithiol molecules as an assembling agent and coated with a CdS shell, using picosecond laser pulses of 532 nm, suggesting that laser irradiation can melt or reshape metal nanoparticles without causing any significant perturbations in the surrounding media.[47-50] Because laser irradiation can heat contacting regions selectively,[47,51,52] the laser-induced transformation of metal nanoparticles has provided a controlled mean to modify the shapes of the nanoparticles precisely. The laser-induced welding mechanism of gold NRs encapsulated in a silica shell is not understood, although the laser-induced size and shape alterations of metal nanoparticles in solutions have been explained to occur through melting and vaporization.[53] Nanosecond laser pulses of 1064 nm are selectively absorbed strongly by the hybridized surface-plasmon resonances of linearly assembled gold NRs in a silica shell. Then, the thermalized photon energy of surface-plasmon excitation induces the contacting surfaces of the gold nanorods to fuse and weld together within a silica shell, transforming a silica-coated gold nanochain into a $Au@SiO_2$ core-shell nanowire. This approach of connecting nanostructures to have ohmic contact at room temperature is anticipated to have potential applications in electric nanodevices and functional circuits.[54-56]

While Figure 5a shows the TEM image of gold NRs, Figure 5b displays the TEM image of gold nanochains which have been formed by the linear self-assembly of gold NRs with the addition of isopropanol. This suggests that gold NRs, initially dispersed well in water, have

been connected in an end-to-end orientation to form gold nanochains with the addition of isopropanol. The time evolution of the linear assembly has been monitored by measuring the extinction spectra of Figure 5c. While the longitudinal SPR band of individual gold NRs at 830 nm decreases gradually, a new SPR band arises at 1100 nm due to the formation of gold nanochains after adding isopropanol. The new band results from the coupling of longitudinal surface-plasmon resonances between linearly assembled gold NRs.[23,31] Thus, our results clearly indicate that isopropanol can induce the end-to-end assembly of gold NRs indeed in the absence of any assembling agents.

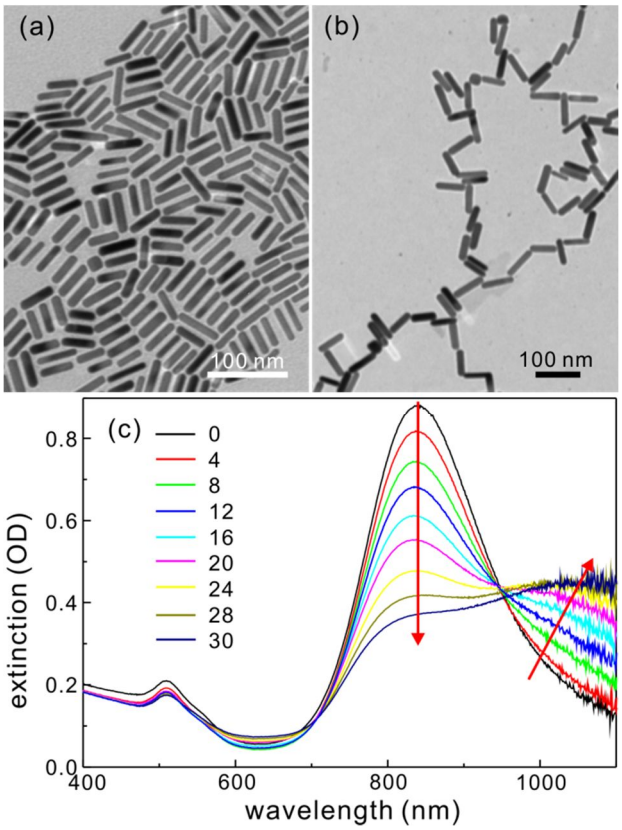

Figure 5. TEM images of (a) gold nanorods and (b) gold nanochains. (c) Extinction spectra of 0.50 mL gold NR colloid recorded as a function of time indicated in the units of min after adding 2.5 mL isopropanol. The arrows indicate the direction of time increase.

It is well-known that cationic CTAB surfactants form a bilayer on the surface of gold NRs, making the NRs positively charged and therefore stabilizing them against aggregation by interparticle electrostatic repulsion. CTAB binds preferentially to the {100} facets of the sides, rather than the {111} facets of the ends, of gold NRs.[28,29,42,57,58] Because the CTAB bilayer is less ordered at the curved ends than on the flat sides, the local density of CTAB is lower at the ends of the NRs than on the sides; the selective binding of assembling agents to the ends of gold NRs has often led to an end-to-end arrangement of gold NRs.[20-28] The CTAB bilayer adsorbed on a gold NR surface is destabilized by adding ethanol, leading CTAB to be dissolved in the surrounding medium.[41] With increase in the composition of organic solvent content, the CTAB bilayer structure has been found to collapse to a monolayer, resulting in the loss of CTAB from the surface of the gold NR.[24] In our experiment, the linear self-assembly process of gold NRs was triggered by adding isopropanol to a colloidal aqueous solution of gold NRs, thereby increasing the solubility of CTAB molecules and reducing the CTAB coverage of the rods. Considering that the CTAB bilayer binds to the side surface of a gold NR with large affinity, the positively charged CTAB bilayer along the rod ends is locally destabilized and removed primarily from the end surface of the gold NR by the increase of CTAB solubility to reduce the electrostatic repulsive potential.[41] Further removal and dissolution of adsorbed CTAB molecules into the surrounding environment allows the end surface of a gold NR to have only a CTAB monolayer, leading to the reduction of electrostatic repulsion and increasing the probability for a close approach between the ends of gold NRs by attractive van der Waals forces. As two NRs with a depleted CTAB monolayer on their end surfaces approach toward to each other, chains of CTAB most likely merge to form a new bilayer between the gold NRs, forming an

end-to-end assembly. This restored CTAB bilayer minimizes energy when the CTAB molecules on two neighboring NRs join together.[37] Thus, we suggest that the restabilization of a CTAB bilayer caused by the attractive van der Waals interactions of CTAB chains between the end surfaces of gold NRs plays a key role in the isopropanol-mediated end-to-end self-assembly of gold NRs.

The *in situ* encapsulation of silica onto gold nanochains suspended in 5:1 (v/v) isopropanol and water has been achieved following the Stöber process: the direct deposition of silica onto CTAB-stabilized gold nanoparticles using TEOS as a precursor in the presence of ammonia as a base catalyst.[45] Figure 6a shows that most gold nanorods are assembled in an end-to-end orientation although the lengths of connected gold nanochains are quite diverse. Each of the gold nanochains has been encapsulated separately in a silica shell having typical thickness of 55 nm. The comparison of Figure 6b with the spectrum measured at 30 min after the addition of isopropanol in Figure 5c reveals that the extinction spectrum of gold nanochains changes hardly by silica coating, although the hybridized SPR band of gold nanochains shifts to the red slightly because of increase in the refractive index of the surrounding medium; the refractive indices of water and silica are 1.33 and 1.45, respectively.[38] This demonstrates that the linearly self-assembled structures of gold nanochains remain intact during the immediately following *in situ* silica coating process. It is well known that the composition of a mixed solvent is critical for uniform silica coating onto nanoparticles.[59] The alcohol-rich environment of 5:1 (v/v) isopropanol and water has been found to be very essential not only for the linear assembly of gold NRs but also for the silica coating of gold nanochains. It has been reported that the aging of the initial gold NR solution is important to guarantee the reproducibility of the subsequent steps.[37,41] We have also found that a freshly synthesized gold NR solution does not undergo linear assembly when

isopropanol is added and that the assembly can take place with adding isopropanol when the gold NR solutions have been aged at least for a month. As mentioned above, the CTAB coverage at the ends of the NRs is likely lower and less robust due to the higher curvature of the end surface and decreases with aging. This, in turn, could lead to significant increase in the dissolution rate of CTAB molecules at the ends of the rods, resulting in a faster self-assembly.[37]

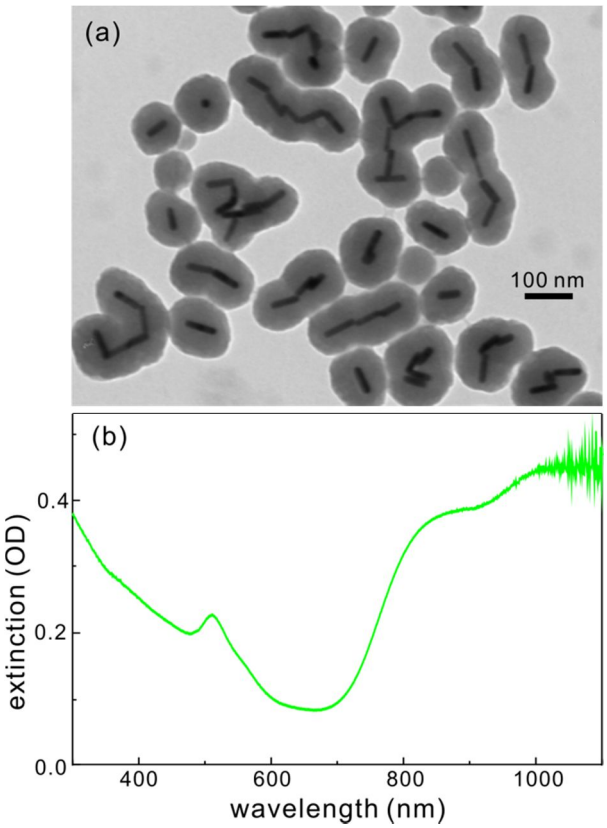

Figure 6. (a) Typical low-magnification TEM image of silica-coated gold nanochains. (b) Extinction spectrum of the nanochains suspended in ethanol.

Silica shells with different thickness have been obtained by controlling the amount of ammonium hydroxide as a base catalyst. The TEM images of Figure 7 show that assembled

gold nanorods encapsulated in silica with average shell thickness values of 20, 35, and 55 nm have been prepared by adding 0.45, 0.48, and 0.50 mL of ammonium hydroxide, respectively, suggesting that the concentration of ammonium hydroxide in the sol-gel process plays an important role in controlling the deposition thickness of silica on gold NRs.[45,60] As the concentration of ammonium hydroxide increases, the silica shell thickness of Au@SiO_2 core-shell nanocomposites increases because the hydrolysis of TEOS requires hydroxide ions provided by ammonium hydroxide;[61] a high concentration of hydroxide ions hydrolyzes TEOS more readily, thus resulting in fast nucleation of silica to form smooth and uniform silica shells.[62]

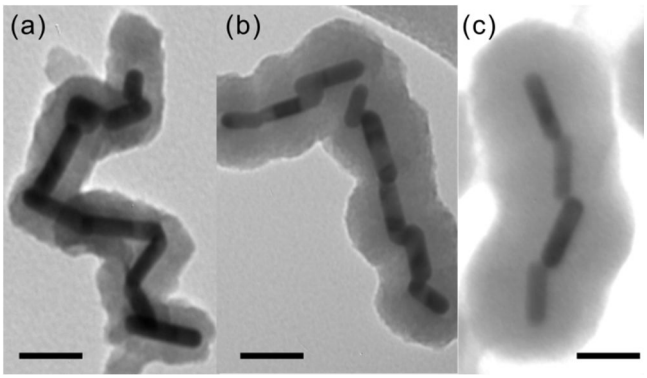

Figure 7. TEM images of silica-coated gold nanochains with shell thickness values of (a) 20 nm, (b) 35 nm, and (c) 55 nm. Each scale bar indicates 50 nm.

2.5. Conclusions

$Au@SiO_2$ core-shell nanowires have been fabricated at room temperature simply by irradiating infrared nanosecond pulses to linearly self-assembled and silica-coated gold nanorods just for 5 min. Gold nanorods have been self-assembled linearly by adding isopropanol in the absence of any assembling agents to form gold nanochains. Isopropanol-mediated linear assembly takes place as CTAB monolayer molecules on the end surfaces of gold nanorods tend to form a bilayer for the enhancement of colloidal stability. Then, the end-to-end assembled gold nanorods have been directly encapsulated with uniform silica shells having tunable thickness to produce silica-coated gold nanochains. It has been found that isopropanol can not only induce the linear assembly of gold NRs but also provide co-solvent environment, which is important to direct silica coating on CTAB-stabilized gold nanochains. The thickness of a silica shell has been controlled by adjusting the supplied amount of ammonia hydroxide. The irradiation of the nanostructures loaded on a TEM grid with nanosecond laser pulses of 1064 nm at fluence of 0.38 mJ/cm^2 has produced $Au@SiO_2$ core-shell nanowires. Laser pulses, selectively absorbed by the hybridized surface-plasmon resonances of linearly assembled gold nanorods in silica shells, are thermalized to heat selectively the contacting surfaces of the gold nanorods, which then fuse and weld together. This is a novel and straightforward synthetic approach for the production of silica-coated gold nanowires having strong near-infrared absorption, high stability, and easily functionalizable surface.

2.6. Acknowledgement

This work was supported by research grants through the National Research Foundation of Korea (NRF) funded by the Korea government (2012-006345 and 2011-0028981). D.J.J. is also thankful to the SRC program of NRF (2007-0056095).

2.7. References

[1] Kim, Y.; Jang, D.-J. Direct Observation of Valence Band Splitting Using Room Temperature Photoluminescence of CdS Hollow Submicrospheres. *Chem. Commun.* **2013,** *49*, 8940-8942.

[2] Kim, J.-Y.; Lee, D.; Kim, H. J.; Lim, I.; Lee, W. I.; Jang, D.-J. Annealing-Free Preparation of Anatase TiO_2 Nanopopcorns on Ti Foil via a Hydrothermal Process and Their Photocatalytic and Photovoltaic Applications. *J. Mater. Chem. A* **2013,** *1*, 5982-5988.

[3] Kim, Y.; Kim, J.-Y.; Jang, D.-J. One-Pot and Template-Free Fabrication of ZnS·(ethylenediamine)$_{0.5}$ Hybrid Nanobelts. *J. Phys. Chem. C* **2012,** *116*, 10296-10302.

[4] Kim, H.-B.; Jang, D.-J. Precursor-Dependent Shape Variation of Wurtzite CdSe Crystals in a Microwave-Assisted Polyol Process. *CrystEngComm* **2012,** *14*, 6946-6951.

[5] Cuenya, B. R. Synthesis and Catalytic Properties of Metal Nanoparticles: Size, Shape, Support, Composition, and Oxidation State Effects. *Thin Solid Films* **2010,** *518*, 3127-3150.

[6] Kwak, J.-A.; Lee, D. K.; Jang, D.-J. Facile Fabrication of Platinum Nanobubbles Having Efficient Catalytic Degradation Performances. *Appl. Catal. B-Environ.* **2013,** *142–143*, 323-328.

[7] Lee, J.; Han, K.; Jang, D.-J. Silica-Coated Silver/Gold Composite Nanoboxes Having Enhanced Catalytic Performances and Reusability. *Appl. Catal. A-Gen.* **2014,** *469*, 380-386.

[8] Rakic, A. D.; Djuri?ic, A. B.; Elazar, J. M.; Majewski, M. L. Optical Properties of Metallic Films for Vertical-Cavity Optoelectronic Devices. *Appl. Opt.* **1998,** *37*, 5271-5283.

[9] Jain, P. K.; Huang, X.; El-Sayed, I. H.; El-Sayed, M. A. Noble Metals on the Nanoscale: Optical and Photothermal Properties and Some Applications in Imaging, Sensing, Biology, and Medicine. *Acc. Chem. Res.* **2008,** *41*, 1578-1586.

[10] Jain, P.; Huang, X.; El-Sayed, I.; El-Sayed, M. Review of Some Interesting Surface Plasmon Resonance-Enhanced Properties of Noble Metal Nanoparticles and Their Applications to Biosystems. *Plasmonics* **2007,** *2*, 107-118.

[11] Shenhar, R.; Rotello, V. M. Nanoparticles: Scaffolds and Building Blocks. *Acc. Chem. Res.* **2003,** *36*, 549-561.

[12] Bifeng, P.; Limei, A.; Feng, G.; Hongye, T.; Rong, H.; Daxiang, C. End-to-End Self-Assembly and Colorimetric Characterization of Gold Nanorods and Nanospheres via

Oligonucleotide Hybridization. *Nanotechnology* **2005,** *16*, 1776-1780.

[13] Yang, P.; Ando, M.; Murase, N. Various Au Nanoparticle Organizations Fabricated through SiO_2 Monomer Induced Self-Assembly. *Langmuir* **2010,** *27*, 895-901.

[14] Chon, J. W. M.; Bullen, C.; Zijlstra, P.; Gu, M. Spectral Encoding on Gold Nanorods Doped in a Silica Sol–Gel Matrix and Its Application to High-Density Optical Data Storage. *Adv. Funct. Mater.* **2007,** *17*, 875-880.

[15] Denisyuk, A. I.; Adamo, G.; MacDonald, K. F.; Edgar, J.; Arnold, M. D.; Myroshnychenko, V.; Ford, M. J.; García de Abajo, F. J.; Zheludev, N. I. Transmitting Hertzian Optical Nanoantenna with Free-Electron Feed. *Nano Lett.* **2010,** *10*, 3250-3252.

[16] Vigderman, L.; Khanal, B. P.; Zubarev, E. R. Functional Gold Nanorods: Synthesis, Self-Assembly, and Sensing Applications. *Adv. Mater.* **2012,** *24*, 4811-4841.

[17] Choi, W.; Sahu, A.; Kim, Y.; Tae, G. Photothermal Cancer Therapy and Imaging Based on Gold Nanorods. *Ann. Biomed. Eng.* **2012,** *40*, 534-546.

[18] Dickerson, E. B.; Dreaden, E. C.; Huang, X.; El-Sayed, I. H.; Chu, H.; Pushpanketh, S.; McDonald, J. F.; El-Sayed, M. A. Gold Nanorod Assisted Near-Infrared Plasmonic Photothermal Therapy (PPTT) of Squamous Cell Carcinoma in Mice. *Cancer Lett.* **2008,** *269*, 57-66.

[19] Chen, Y.-S.; Frey, W.; Kim, S.; Homan, K.; Kruizinga, P.; Sokolov, K.; Emelianov, S. Enhanced Thermal Stability of Silica-Coated Gold Nanorods for Photoacoustic Imaging and Image-Guided Therapy. *Opt. Express* **2010,** *18*, 8867-8878.

[20] Zhang, S.; Kou, X.; Yang, Z.; Shi, Q.; Stucky, G. D.; Sun, L.; Wang, J.; Yan, C. Nanonecklaces Assembled from Gold Rods, Spheres, and Bipyramids. *Chem. Commun.* **2007,** *18*, 1816-1818.

[21] Sun, Z.; Ni, W.; Yang, Z.; Kou, X.; Li, L.; Wang, J. pH-Controlled Reversible Assembly and Disassembly of Gold Nanorods. *Small* **2008,** *4*, 1287-1292.

[22] Nie, Z.; Fava, D.; Kumacheva, E.; Zou, S.; Walker, G. C.; Rubinstein, M. Self-Assembly of Metal-Polymer Analogues of Amphiphilic Triblock Copolymers. *Nat. Mater.* **2007,** *6*, 609-614.

[23] Thomas, K. G.; Barazzouk, S.; Ipe, B. I.; Joseph, S. T. S.; Kamat, P. V. Uniaxial Plasmon Coupling through Longitudinal Self-Assembly of Gold Nanorods. *J. Phys. Chem. B* **2004,** *108*, 13066-13068.

[24] Pramod, P.; Thomas, K. G. Plasmon Coupling in Dimers of Au Nanorods. *Adv. Mater.* **2008,** *20*, 4300-4305.

[25] Shao, L.; Woo, K. C.; Chen, H.; Jin, Z.; Wang, J.; Lin, H.-Q. Angle- and Energy-Resolved Plasmon Coupling in Gold Nanorod Dimers. *ACS Nano* **2010,** *4*, 3053-3062.

[26] Wang, L.; Zhu, Y.; Xu, L.; Chen, W.; Kuang, H.; Liu, L.; Agarwal, A.; Xu, C.; Kotov, N. A. Side-by-Side and End-to-End Gold Nanorod Assemblies for Environmental Toxin Sensing. *Angew. Chem. Int. Ed.* **2010,** *49*, 5472-5475.

[27] Wang, Y.; Li, Y. F.; Wang, J.; Sang, Y.; Huang, C. Z. End-to-End Assembly of Gold Nanorods by Means of Oligonucleotide-Mercury(II) Molecular Recognition. *Chem. Commun.* **2010,** *46*, 1332-1334.

[28] Jain, T.; Roodbeen, R.; Reeler, N. E. A.; Vosch, T.; Jensen, K. J.; Bjørnholm, T.; Nørgaard, K. End-to-End Assembly of Gold Nanorods via Oligopeptide Linking and Surfactant Control. *J. Colloid Interface Sci.* **2012,** *376*, 83-90.

[29] Laza, S. C.; Sanson, N.; Sicard-Roselli, C.; Aghedu, A.; Palpant, B. Selective Cold Welding of Colloidal Gold Nanorods. *Part. Part. Syst. Charact.* **2013,** *30*, 584-589.

[30] Maier, S. A.; Kik, P. G.; Atwater, H. A.; Meltzer, S.; Harel, E.; Koel, B. E.; Requicha, A. A. G. Local Detection of Electromagnetic Energy Transport Below the Diffraction Limit in Metal Nanoparticle Plasmon Waveguides. *Nat. Mater.* **2003,** *2*, 229-232.

[31] Aizpurua, J.; Bryant, G. W.; Richter, L. J.; García de Abajo, F. J.; Kelley, B. K.; Mallouk, T. Optical Properties of Coupled Metallic Nanorods for Field-Enhanced Spectroscopy. *Phys. Rev. B* **2005,** *71*, 235420.

[32] Ko, H.; Singamaneni, S.; Tsukruk, V. V. Nanostructured Surfaces and Assemblies as SERS Media. *Small* **2008,** *4*, 1576-1599.

[33] Huang, X.; Neretina, S.; El-Sayed, M. A. Gold Nanorods: From Synthesis and Properties to Biological and Biomedical Applications. *Adv. Mater.* **2009,** *21*, 4880-4910.

[34] Tucker-Schwartz, J. M.; Meyer, T. A.; Patil, C. A.; Duvall, C. L.; Skala, M. C. In Vivo Photothermal Optical Coherence Tomography of Gold Nanorod Contrast Agents. *Biomed. Opt. Express* **2012,** *3*, 2881-2895.

[35] Wijaya, A.; Schaffer, S. B.; Pallares, I. G.; Hamad-Schifferli, K. Selective Release of Multiple DNA Oligonucleotides from Gold Nanorods. *ACS Nano* **2008,** *3*, 80-86.

[36] Tang, H.; Kobayashi, H.; Niidome, Y.; Mori, T.; Katayama, Y.; Niidome, T. CW/Pulsed

NIR Irradiation of Gold Nanorods: Effect on Transdermal Protein Delivery Mediated by Photothermal Ablation. *J. Control. Release* **2013,** *171*, 178-183.

[37] Wang, Y.; DePrince, A. E.; K. Gray, S.; Lin, X.-M.; Pelton, M. Solvent-Mediated End-to-End Assembly of Gold Nanorods. *J. Phys. Chem. Lett.* **2010,** *1*, 2692-2698.

[38] Cho, E. C.; Choi, S.-W.; Camargo, P. H. C.; Xia, Y. Thiol-Induced Assembly of Au Nanoparticles into Chainlike Structures and Their Fixing by Encapsulation in Silica Shells or Gelatin Microspheres. *Langmuir* **2010,** *26*, 10005-10012.

[39] Roca, M.; Pandya, N. H.; Nath, S.; Haes, A. J. Linear Assembly of Gold Nanoparticle Clusters via Centrifugation. *Langmuir* **2010**, *26*, 2035-2041.

[40] Yang, M.; Chen, G.; Zhao, Y.; Silber, G.; Wang, Y.; Xing, S.; Han, Y.; Chen, H. Mechanistic Investigation into the Spontaneous Linear Assembly of Gold Nanospheres. *Phys. Chem. Chem. Phys.* **2010,** *12*, 11850-11860.

[41] Nepal, D.; Park, K.; Vaia, R. A. High-Yield Assembly of Soluble and Stable Gold Nanorod Pairs for High-Temperature Plasmonics. *Small* **2012,** *8*, 1013-1020.

[42] Sun, Z.; Bao, Z.; Fang, C.; Wang, J. Formation of Different Gold Nanocrystal Core–Resin Shell Structures through the Control of the Core Assembly and Shell Polymerization. *Langmuir* **2012,** *28*, 9082-9092.

[43] Annan, W.; Qing, P.; Yadong, L. Rod-Shaped Au–Pd Core–Shell Nanostructures. *Chem. Mater.* **2011,** *23*, 3217-3222.

[44] Orendorff, C. J.; Murphy, C. J. Quantitation of Metal Content in the Silver-Assisted Growth of Gold Nanorods. *J. Phys. Chem. B* **2006,** *110*, 3990-3994.

[45] Cong, H.; Toftegaard, R.; Arnbjerg, J.; Ogilby, P. R. Silica-Coated Gold Nanorods with a Gold Overcoat: Controlling Optical Properties by Controlling the Dimensions of a Gold−Silica−Gold Layered Nanoparticle. *Langmuir* **2009,** *26*, 4188-4195.

[46] Kim, J.-Y.; Kim, S. J.; Jang, D.-J. Laser-Induced Fabrication of Au@CdS Core−Shell Nanowires. *J. Phys. Chem. C* **2010,** *115*, 672-675.

[47] Kim, S. J.; Jang, D.-J. Laser-Induced Nanowelding of Gold Nanoparticles. *Appl. Phys. Lett.* **2005,** *86*, 033112.

[48] Ah, C. S.; Kim, S. J.; Jang, D.-J. Laser-Induced Mutual Transposition of the Core and the Shell of a Au@Pt Nanosphere. *J. Phys. Chem. B* **2006,** *110*, 5486-5489.

[49] Petrova, H.; Lin, C.-H.; Hu, M.; Chen, J.; Siekkinen, A. R.; Xia, Y.; Sader, J. E.;

Hartland, G. V. Vibrational Response of Au−Ag Nanoboxes and Nanocages to Ultrafast Laser-Induced Heating. *Nano Lett.* **2007,** *7*, 1059-1063.

[50] Harada, M.; Okamoto, K.; Terazima, M. Diffusion of Gold Ions and Gold Particles during Photoreduction Processes Probed by the Transient Grating Method. *J. Colloid Interface Sci.* **2009,** *332*, 373-381.

[51] Garnett, E. C.; Cai, W.; Cha, J. J.; Mahmood, F.; Connor, S. T.; Greyson Christoforo, M.; Cui, Y.; McGehee, M. D.; Brongersma, M. L. Self-Limited Plasmonic Welding of Silver Nanowire Junctions. *Nat. Mater.* **2012,** *11*, 241-249.

[52] Son, M.; Kim, S. J.; Kim, J.-Y.; Jang, D.-J. Laser-Induced Silver Nanojoining of Gold Nanoparticles. *J. Nanosci. Nanotechnol.* **2013,** *13*, 5777-5782.

[53] Hartland, G. V. Coherent Excitation of Vibrational Modes in Metallic Nanoparticles. *Annu. Rev. Phys. Chem.* **2006,** *57*, 403-430.

[54] Dong; Tao; Zhang, L.; Zhang; Nelson, B. J. Nanorobotic Spot Welding: Controlled Metal Deposition with Attogram Precision from Copper-Filled Carbon Nanotubes. *Nano Lett.* **2006,** *7*, 58-63.

[55] Lu, Y.; Huang, J. Y.; Wang, C.; Sun, S.; Lou, J. Cold Welding of Ultrathin Gold Nanowires. *Nat. Nanotechnol.* **2010,** *5*, 218-224.

[56] Singh, S. C.; Gopal, R. Drop Shaped Zinc Oxide Quantum Dots and Their Self-Assembly into Dendritic Nanostructures: Liquid Assisted Pulsed Laser Ablation and Characterizations. *Appl. Surf. Sci.* **2012,** *258*, 2211-2218.

[57] Kawamura, G.; Yang, Y.; Nogami, M. Facile Assembling of Gold Nanorods with Large Aspect Ratio and Their Surface-Enhanced Raman Scattering Properties. *Appl. Phys. Lett.* **2007,** *90*, 261908.

[58] Lee, S.; Anderson, L. J. E.; Payne, C. M.; Hafner, J. H. Structural Transition in the Surfactant Layer that Surrounds Gold Nanorods as Observed by Analytical Surface-Enhanced Raman Spectroscopy. *Langmuir* **2011,** *27*, 14748-14756.

[59] Nooney, R. I.; Thirunavukkarasu, D.; Chen, Y.; Josephs, R.; Ostafin, A. E. Self-Assembly of Mesoporous Nanoscale Silica/Gold Composites. *Langmuir* **2003,** *19*, 7628-7637.

[60] Mine, E.; Yamada, A.; Kobayashi, Y.; Konno, M.; Liz-Marzán, L. M. Direct Coating of Gold Nanoparticles with Silica by a Seeded Polymerization Technique. *J. Colloid Interface Sci.* **2003,** *264*, 385-390.

[61] Pak, J.; Yoo, H. Facile Synthesis of Spherical Nanoparticles with a Silica Shell and Multiple Au Nanodots as the Core. *J. Mater. Chem. A* **2013,** *1*, 5408-5413.
[62] Huang, C.-C.; Huang, C.-H.; Kuo, I. T.; Chau, L.-K.; Yang, T.-S. Synthesis of Silica-Coated Gold Nanorod as Raman Tags by Modulating Cetyltrimethylammonium Bromide Concentration. *Colloids Surf. Physicochem. Eng. Aspects* **2012,** *409*, 61-68.

Appendicies

A.1. List of Publications

1. **Myounghee Son**, Seol Ji Kim, Jong-Yeob Kim, and Du-Jeon Jang, "Laser-Induced Silver Nanojoining of Gold Nanoparticles" J. Nanosci. Nanotech. 2013, 13, 5777–5782.
2. **Myounghee Son**, Jaewon Lee, and Du-Jeon Jang, "Light-treated silica-coated gold nanorods having highly enhanced catalytic performances and reusability" J. Mol. Catal. A: Chem. submitted.
3. **Myounghee Son**, Sookyung Jung, and Du-Jeon Jang, "Laser-Induced Welding of Self-Assembled Gold Nanorods to Fabricate Au@SiO_2 Core-Shell Nanowires" to be submitted.

A.2. List of Presentations

A.2.1. International Presentation

1. Jong-Yeob Kim, **Myounghee Son**, and Du-Jeon Jang, "ZnO Nanowires Fabricated Hydrothermally for Room-Temperature Ultraviolet Nanolasers", *Gordon Research Conferences on Colloidal, Macromolecular & Polyelectrolyte Solutions*, Ventura, CA, USA (**2012**).

A.2.2. Domestic Presentation

1. **Myounghee Son**, Seol-Ji Kim, Jong-Yeob Kim, and Du-Jeon Jang, "Laser-Induced Silver Nanosoldering of Gold Nanoparticles", *The 108th Autumn Meeting of the Korean Chemical Society*, Deajeon, Korea (**2011**).

2. **Myounghee Son** and Du-Jeon Jang, "Gold Nanoparticles Silver-Nanosoldered by Laser Irradiation", *The 109th Spring Meeting of the Korean Chemical Society*, Goyang, Korea (**2012**).

3. **Myounghee Son**, Jong-Yeob Kim, and Du-Jeon Jang, "One-pot synthesis of Au@SiO_2 core-shell nanochains", *The 110th Autumn Meeting of the Korean Chemical Society*, Busan, Korea (**2012**).

Abstract (Korean)

금 나노막대에 실리카 쉘을 쌓은 나노구조체에 나노초 펄스 레이저나 제논 램프를 조사하여 제작된 구조가, 기존의 구조보다 더 나은 광학적, 구조적, 촉매적 특성을 지님을 연구하였다. 제조한 나노구조체의 특성은 전자 현미경 이미지와 시간 의존적 자외선-가시광선 영역 흡수 분광학을 이용하여 분석하고 평가하였다.

1장에서는 다공성의 실리카가 코팅된 금 나노막대에 제논 램프를 조사하여, 조사 전보다 4-nitropheonl의 환원반응에 대하여 향상된 촉매 활성을 가짐을 확인하였다. 다공성 실리카가 코팅된 금 나노막대를 고해상도 전자현미경으로 관찰한 구조는 빛 처리를 한 후에도 변화가 없었지만, 촉매반응성과 재사용성은 증가됨이 관찰되었다. 빛을 조사하면 금 나노막대의 광열효과에 의하여 막대 표면 원자들의 재구조화가 일어나게 되고, 이로 인하여 촉매 반응이 일어나는 금 표면에 반응 분자들이 더욱 쉽게 흡착될 뿐만 아니라, 촉매 반응의 키네틱 장벽을 낮추기 때문에 촉매 반응의 전자 전달의 속도가 증가되어 촉매반응성이 증가된다는 것을 표면 플라즈몬 공명의 변화를 통해 설명하였다.

2장에서는 실리카 쉘을 쌓은 자기조립된 금 나노막대 구조체에 나노 초 펄스 레이저를 조사하여 나노 막대를 접합시킨 나노와이어 구조체의 제조에 대해 논하였다. 기존에 보고된 금 나노막대의 자기조립에는 조립을 시켜주는 접합물질이 필요하지만, 본 연구에서는 접합물질 없이도 isopropanol 용매와 계면활성제 Cetyltrimethyl ammonium bromide의 작용에 의해 막대의 끝과 끝이

연결되는 자기조립이 유도된다는 사실을 처음으로 밝혔다. 또한 이 구조체를 용액상에서 안정화시키기 위한 실리카 쉘을 쌓는 최적의 합성 조건을 제시하였다. 나노 초 레이저를 조사하여 자기조립된 금 나노막대가 전기적인 옴 접촉을 가지는 금 나노 와이어 구조체를 제조하였다.

주요어: 귀금속, 금, 나노막대, 레이저 접합, 빛 처리, 자기조립 촉매, 코어-쉘

학번: 2011-20295